Fluctuation-dissipation relations in the nonequilibrium critical dynamics of Ising models

Peter Mayer,[1] Ludovic Berthier,[2,3] Juan P. Garrahan,[2] and Peter Sollich[1]
[1]*Department of Mathematics, King's College, Strand, London WC2R 2LS, United Kingdom*
[2]*Theoretical Physics, University of Oxford, 1 Keble Road, Oxford OX1 3NP, United Kingdom*
[3]*Laboratoire des Verres, Université Montpellier II, 34095 Montpellier, France*
(Received 28 January 2003; published 21 July 2003)

We investigate the relation between two-time multispin correlation and response functions in the nonequilibrium critical dynamics of Ising models in $d=1$ and $d=2$ spatial dimensions. In these nonequilibrium situations, the fluctuation-dissipation theorem (FDT) is not satisfied. We find FDT ''violations'' qualitatively similar to those reported in various glassy materials, but quantitatively dependent on the chosen observable, in contrast to the results obtained in infinite-range glass models. Nevertheless, all FDT violations can be understood by considering separately the contributions from large wave vectors, which are at quasiequilibrium and obey the FDT, and from small wave vectors where a generalized FDT holds with a nontrivial fluctuation-dissipation ratio X^∞. In $d=1$, we get $X^\infty=\frac{1}{2}$ for spin observables, which measure the orientation of domains, while $X^\infty=0$ for observables that are sensitive to the domain-wall motion. Numerical simulations in $d=2$ reveal a unique $X^\infty\simeq 0.34$ for all observables. Measurement protocols for X^∞ are discussed in detail. Our results suggest that the definition of an effective temperature $T_{\rm eff}=T/X^\infty$ for large length scales is generically possible in nonequilibrium critical dynamics.

DOI: 10.1103/PhysRevE.68.016116 PACS number(s): 05.70.Ln, 75.40.Gb, 75.40.Mg

INTRODUCTION

Since the analytical solution of the nonequilibrium dynamics of the spherical *p*-spin model in its low temperature phase [1], many studies have focused on the properties of two-time nonequilibrium correlation and response functions, and the relationship between them [2,3]. In this paper, we report on analytical and numerical investigations of several two-time multispin correlation and response functions in the nonequilibrium critical dynamics of Ising models in $d=1$ and $d=2$ spatial dimensions.

Our work is motivated by the following observations. Multipoint dynamical functions are standard objects in equilibrium statistical mechanics which reveal microscopic information related to experimentally observable quantities. In nonequilibrated systems, however, the equilibrium relation between response and correlation, i.e., the fluctuation-dissipation theorem (FDT), is not satisfied. This evident observation became important when it was realized that in the *p*-spin model [1] and more generally in infinite-range glass models, a *generalized* FDT can be formulated [2–5]. This amounts to the introduction of a fluctuation-dissipation ratio X or, alternatively, of an effective temperature $T_{\rm eff}=T/X$ for the slow, nonequilibrated modes of the system [6]. The properties of X and $T_{\rm eff}$ have attracted much interest, since they suggest that a generalized statistical mechanics can be devised to deal with a broad class of nonequilibrium phenomena.

The generalized FDT is exact for infinite-range glass models only. It is, however, tempting to apply the same concepts in other contexts such as glassy systems with finite interaction range, as observed experimentally or simulated numerically. A further step is made when those ideas are transferred to other physical situations such as domain growth processes [7,8] in nondisordered systems or the rheology of soft glassy materials [9,10]. Although one does not expect the results for infinite-range glass models to apply exactly in all these nonequilibrium situations, it is worthwhile to understand analogies and differences, and thus to push these ideas as far as possible. This is the philosophy of our paper where nonequilibrium dynamics at criticality is analyzed along the lines described above. Our results suggest that the concept of a generalized FDT is indeed useful at criticality, and we describe in detail the form it takes as compared to the results obtained in infinite-range glass models.

The manuscript is organized as follows. The first section below reviews the results obtained for correlation and response functions in ferromagnets and delineates the scope of the paper. In Sec. II, the $1d$ Ising model is studied analytically at $T_c=0$. In Sec. III, numerical results for the $2d$ Ising model at T_c are presented. A summary and a physical discussion of the results can be found in the last section.

I. FDT AND FERROMAGNETS

A. Correlation and response functions

Pure ferromagnets are generally not described as glassy materials, which are loosely defined as systems with large relaxation times. However, if a ferromagnet initially prepared at high temperature is suddenly quenched to its low temperature ferromagnetic phase, its equilibration time diverges with system size [11]. This is true also when the quench is performed precisely to the critical point, $T=T_c$. In both cases the system remains, in the thermodynamic limit, forever in a nonequilibrated, nonstationary state: it exhibits aging. Therefore, one can study physical situations in pure ferromagnets that are reminiscent of aging phenomena observed, e.g., in spin glasses, polymers, or colloids. One is then led to ask if the tools used in the glass literature are also useful to describe this type of nonequilibrium situation.

These tools include, in particular, two-time correlation and response functions. Consider two physical observables

$A(t)$ and $B(t)$. Their connected cross correlation is defined by

$$C(t,t_w)=\langle A(t)B(t_w)\rangle-\langle A(t)\rangle\langle B(t_w)\rangle, \tag{1}$$

while the conjugate response function is given by

$$R(t,t_w)=T\left.\frac{\delta\langle A(t)\rangle}{\delta h_B(t_w)}\right|_{h_B=0}. \tag{2}$$

Here h_B is the thermodynamically conjugate field to the observable B; for later convenience we scale the response by T. Numerically or experimentally, it is often more convenient to measure the integrated response function, or susceptibility,

$$\chi(t,t_w)=\int_{t_w}^{t} d\tau R(t,\tau), \tag{3}$$

which gives the response to a small constant field h_B switched on at the ''waiting time'' t_w.

At equilibrium, correlation and response are time-translation invariant and related by the FDT

$$R(t,t_w)=\frac{\partial}{\partial t_w}C(t,t_w). \tag{4}$$

In that case, $\langle\cdots\rangle$ in Eqs. (1) and (2) stands for the usual ensemble average. If one follows instead the dynamics of the system after a sudden quench, the system is out of equilibrium and neither the time-translation invariance nor the FDT is satisfied. Then $\langle\cdots\rangle$ is to be read as an average over initial conditions and any stochasticity in the dynamics. In infinite-range glass models, a generalized FDT is satisfied in the aging dynamics. The generalization amounts to the introduction of a fluctuation-dissipation ratio (FDR), $X(t,t_w)$, through

$$-\frac{\partial}{\partial t_w}\chi(t,t_w)=R(t,t_w)=X(t,t_w)\frac{\partial}{\partial t_w}C(t,t_w). \tag{5}$$

This definition becomes nontrivial because in the limit of long times t and t_w, the FDR reduces to a function of a single variable only, namely, the correlation function,

$$X(t,t_w)\to X(C(t,t_w)), \tag{6}$$

where we retain the same symbol for the FDR and its long-time limit. As in equilibrium, response and correlation are then no longer independent quantities, although their relationship is now more complex.

It is now standard to study this generalized FDT via the parametric representation, or ''FD plot,'' of the susceptibility χ as a function of the correlation C [4]. At equilibrium, one has $\chi(t,t_w)=C(t,t)-C(t,t_w)$. Hence, a plot of $\chi(t,t_w)$ against $C(t,t)-C(t,t_w)$ gives a simple straight line of slope 1: this is the equilibrium FD plot. Out of equilibrium, Eq. (6) implies

$$\chi(t,t_w)=\int_{C(t,t_w)}^{C(t,t)} dx X(x). \tag{7}$$

Therefore, when Eq. (6) holds, the FDR can be obtained directly from the slope of the FD plot, which is $X(C)$. Otherwise, from Eq. (5) a plot of $\chi(t,t_w)$ against $C(t,t)-C(t,t_w)$, with t fixed and t_w the curve parameter, will still have slope $X(t,t_w)$. Since the amplitude of correlation and response functions can diverge or converge to zero for $t\to\infty$ (see below) it can be useful to use normalized quantities, plotting $\tilde{\chi}(t,t_w)\equiv\chi(t,t_w)/C(t,t)$ versus $1-\tilde{C}(t,t_w)$ where $\tilde{C}(t,t_w)=C(t,t_w)/C(t,t)$. Since the normalization factors are independent of t_w, the slope of the FD plot is then still given by X. The normalization issue is less important when presenting numerical data, which are by construction obtained in a restricted time window where the amplitudes of the dynamical quantities typically change only slowly.

Appealingly, the FDR can also be interpreted as defining an effective temperature, $T_{\rm eff}(t,t_w)\equiv T/X(t,t_w)$, replacing the equilibrium temperature T by an equivalent quantity out of equilibrium. Moreover, it is a general result that for the case $A=B$, where one considers the autocorrelation of A and the associated response, $T_{\rm eff}$ is the temperature measured by a thermometer coupled to the observable A at the appropriate time scale [6]. As a direct corollary, this effective temperature then satisfies the zeroth law of thermodynamics. Clearly, however, the introduction of an effective temperature is of thermodynamic interest only if $T_{\rm eff}$ is actually independent of the observables A and B under consideration. This is indeed true for infinite-range glass models [6], implying that although the system is out of equilibrium it can still be described in thermodynamic terms, at the moderate cost of introducing one extra parameter, namely, the effective temperature [12]. Beyond infinite-range glass models, the observable dependence of the effective temperature remains largely an open question but has been discussed in detail in the context of trap models [13] and in a realistic numerical model of a supercooled liquid [14].

B. Ferromagnets at low temperature

For ferromagnets, two-time dynamical functions have been studied both for a quench to the low temperature phase and to criticality, with most work to date focused on the first situation.

In the low temperature phase, the evolution of the system consists in the growth of ordered domains, with a typical domain size $\ell(t)$. Two-time quantities that have been thoroughly studied are the spin-autocorrelation function $C_s(t,t_w)=\langle s_i(t)s_i(t_w)\rangle$, where $s_i(t)$ is the value of the spin at site i at time t, and the conjugate response function $R_s(t,t_w)=-(\partial/\partial t_w)\chi_s(t,t_w)=\delta\langle s_i(t)\rangle/\delta h_i(t_w)$, where h_i is the magnetic field at site i. In this case, the connected and disconnected correlations coincide, since $\langle s_i(t)\rangle=0$ at all stages of the coarsening process. From the analytical solution of solvable models [15–19] and the simulation of more realistic situations [7,8,20–22], the behavior of these two quantities is now well known. For small time differences, $\Delta t=t-t_w\ll t_w$, time-translation invariant behavior is observed, $C_s(t,t_w)\approx C_s(\Delta t)$, $\chi_s(t,t_w)\approx\chi_s(\Delta t)$, and the FDT $\chi_s(t,t_w)\approx C_s(t,t)-C_s(t,t_w)$ is obeyed. This first regime is

due to thermal fluctuations in the bulk of the domains, which are essentially equilibrium fluctuations. For larger time separations, $\Delta t \gg t_w$, the fluctuations of the interfaces dominate the dynamical behavior. The reasonable hypothesis that coarsening is a self-similar process, in the sense that for large times all dynamical functions depend on time only through the typical domain size ℓ, implies the scaling form $C_s(t,t_w) \approx C_s(\ell(t)/\ell(t_w))$ for the correlation function. The contribution of the interfaces to the response function can be estimated [8] as a sum over all wave vectors, $\chi_s(t,t_w) \approx \int_{1/\ell(t_w)}^{1/a} d^d\mathbf{k} k^{-2} \ell^{-1}(t)$. This expression results from the fact that the response at time t_w is dominated by large wave vectors, $k\ell(t_w) \gg 1$, each wave vector $\mathbf{k}$ giving a contribution of the order of k^{-2}. The factor $\ell^{-1}(t)$ represents the density of domain walls, and a is a UV cutoff given by the lattice spacing. This reasoning implies for the long-time contribution to the susceptibility the scaling form $\chi_s(t,t_w) \approx f(\ell(t_w))\chi_s(\ell(t)/\ell(t_w))$, where the function $f(x)$ depends on the dimensionality d of space and is given by $f(x)=1/x$ for $d>2$, $f(x)=(\ln x)/x$ for $d=2$ and $f(x)=$ const for $d=1$. This scaling function has recently been revisited in Refs. [22,23], with particular attention to the case $d=2$ [24,25].

From the above arguments, and for $d>1$, the parametric plot of $\chi_s(t,t_w)$ versus $C_s(t,t_w)-C_s(t,t_w)$ consists of an initial equilibrium part followed by an essentially horizontal section. In the latter the correlation function decays due to interface motion, while the response function hardly changes because any contribution from the interfaces is suppressed by the $f(\ell(t_w))$ prefactor. If a limiting FDR X_s^∞ is defined through

$$X_s^\infty = \lim_{t_w\to\infty} \lim_{t\to\infty} X_s(t,t_w), \tag{8}$$

then it follows that $X_s^\infty = 0$ for $d>1$ in coarsening processes. For $d=1$, on the other hand, both χ_s and C_s are scaling functions of $\ell(t)/\ell(t_w)$ and the parametric plot assumes no simple shape, implying that X_s^∞ could be any finite number. This is confirmed by the analytical solution of the dynamics of the Ising chain at $T=0$ which shows that $X_s^\infty = \frac{1}{2}$ [26,27]. The factor $\frac{1}{2}$ was first derived in Ref. [28].

C. Ferromagnets at the critical point

The nontrivial value of X_s^∞ for the Ising chain was interpreted using the fact that in $d=1$, the ordering temperature $T=0$ coincides with the critical point $T_c=0$ [26]. It was then suggested that a nontrivial X_s^∞ could be a generic feature of critical points [29]. This is physically reasonable, since the whole argument for $X_s^\infty=0$ in coarsening processes relies on the separation between bulk and interfaces; this is no longer valid at the critical point where the bulk has the well-known self-similar structure of ferromagnets at criticality.

From analytical and numerical studies, the behavior of two-time single-spin dynamical quantities is again well understood, as briefly reviewed in Ref. [30]. Physically, the nonequilibrium dynamics following a quench to the critical point consists in the growth of the dynamical correlation length, $\xi(t) \approx t^{1/z}$, where z is the dynamical critical exponent [31]. Critical fluctuations of large wave vectors, $k\xi(t) \gg 1$, are almost equilibrated, while those with small wave vectors, $k\xi(t) \ll 1$, still retain their nonequilibrium initial condition. This separation leads to the scaling forms $C_s(t,t_w) \approx \Delta t^{-2\beta/\nu z} C_s(\xi(t)/\xi(t_w))$ and $\chi_s(t,t_w) \approx \Delta t^{-2\beta/\nu z} \chi_s(\xi(t)/\xi(t_w))$, where β and ν are the standard critical exponents. This can be interpreted as follows. For short-time differences $\Delta t \ll t_w$, equilibrated fluctuations with large k dominate and dynamical functions assume their standard equilibrium power-law decay. The dynamics at large time separation $\Delta t \gg t_w$, on the other hand, is dominated by the growth of the dynamic correlation length and leads to the $\xi(t)/\xi(t_w)$ scaling. This in turn implies that, beyond the initial equilibrium part, the FD plot will again assume a nontrivial shape, as in the Ising chain. The striking similarity of these results with the aging dynamics of finite dimensional spin glasses was noted in Refs. [29,32].

The reasoning above confirms that at criticality, X_s^∞ can take any finite value, in contrast with the $X_s^\infty=0$ obtained in the low temperature phase. It was further argued that X_s^∞ should be a new universal quantity at criticality [29]. As such, it can be computed using standard renormalization group procedures, and this program has recently been started for various models [33–35]. The value of X_s^∞ is known exactly for the Ising chain [26–28], where $X_s^\infty = \frac{1}{2}$, for the spherical ferromagnetic model [29], where $X_s^\infty = \frac{1}{2}$ for $d \geq 4$ and $X_s^\infty = \frac{1}{3}$ for $d=3$, and for the Gaussian model [15] where $X_s^\infty = \frac{1}{2}$. An estimate is known for model A at second order in $4-d$ [33], to first order in $\sqrt{4-d}$ for the diluted Ising model [34], and to first order in $4-d$ in model C [35].

D. Motivations for this work

This short review of known results in the nonequilibrium dynamics of pure ferromagnets shows that much research has been done on the subject. So, why another paper?

First of all, the relevance of the notion of an effective temperature at criticality can be questioned because the FD plots for the spin dynamic functions do not assume a simple linear shape with a well-defined slope, as happens in the low temperature phase. This is related to the fact that at low temperatures the decay of correlation functions occurs on two well-separated time scales. Each has its own associated effective temperature, a fact reminiscent of the physics of structural glasses. At criticality, on the other hand, one has a continuum of time scales associated with different wave vectors, $t(k) \sim k^{-z}$. Moreover, for finite k the equilibration time is finite, meaning that the number of modes that are still out of equilibrium decreases as time increases. This suggests that an effective temperature could be relevant only when considering the $k \to 0$ limit, a point which our analysis will clarify.

Second, we mentioned the important issue of the observable dependence of a generalized FDT. This issue remains completely open since the studies cited above focused exclusively on a single FD relation, for the spin autocorrelation and associated response. In order to get a more complete theoretical understanding, it is crucial to understand if other

observables give the same results, and if not, how they are related.

A third motivation for the study of higher-order correlation functions comes from the observation that the dynamics of coarsening models is dominated by the motion of topological defects. For Ising models, these are domain walls, the local density of which is given by the ''defect'' observable $s_i(t)s_j(t)$, where (i,j) are nearest neighbors. Defect dynamical functions have recently been studied in the context of kinetically constrained Ising models [36], and the FD relations that arose showed interesting and unexpected features.

For an Ising model, there are at least four ''natural'' FD relations, involving, respectively, the spin autocorrelation $C_{\rm s}(t,t_{\rm w})$, the magnetization density $m(t)$ correlation, $C_{\rm m}(t,t_{\rm w})=\langle m(t)m(t_{\rm w})\rangle$, the defect autocorrelation

$$C_{\rm d}(t,t_{\rm w})=\langle s_i(t)s_j(t)s_i(t_{\rm w})s_j(t_{\rm w})\rangle - \langle s_i(t)s_j(t)\rangle\langle s_i(t_{\rm w})s_j(t_{\rm w})\rangle$$

with (i,j) nearest neighbors, and the energy density $e(t)$ correlation $C_{\rm e}(t,t_{\rm w})=\langle e(t)e(t_{\rm w})\rangle-\langle e(t)\rangle\langle e(t_{\rm w})\rangle$. Note again that connected and disconnected correlation functions coincide for the magnetization; this is not the case for $C_{\rm d}(t,t_{\rm w})$ and $C_{\rm e}(t,t_{\rm w})$. In the $1d$ case, we will also investigate two-time functions which smoothly interpolate between incoherent, local functions (spin or defect) and coherent, global ones (magnetization, energy), and discuss the case of correlation functions of higher order. In the $2d$ case, we will stick to the four quantities listed above.

II. THE 1*d* ISING MODEL

In this section, we study the nonequilibrium dynamics in the Glauber-Ising chain with the Hamiltonian

$$\mathcal{H}=-\sum_i s_i s_{i+1}, \tag{9}$$

where the s_i $(i=1,\ldots,N)$ are N Ising spins subject to periodic boundary conditions. Glauber dynamics consists in each spin s_i flipping with rate $\frac{1}{2}[1-\frac{1}{2}\gamma s_i(s_{i-1}+s_{i+1})]$, where $\gamma=\tanh(2/T)$. Equivalently, the flip rates can be written as $1/[1+\exp(\Delta\mathcal{H}/T)]$, where $\Delta\mathcal{H}$ is the change in the Hamiltonian caused by the flip. We use this second expression to extend the definition of the rates to the case where the Hamiltonian includes field terms such as $-\Sigma_i h_i s_i$, following, e.g., Ref. [26]. Glauber's original prescription treated the effects of external fields separately [37] but is less standard today.

We focus on the evolution of arbitrary two-time spin and defect correlation and response functions in the thermodynamic limit $N\to\infty$, after a quench from equilibrium at $T=\infty$ to $T\to 0$. As explained above, although a variety of aspects of the associated coarsening dynamics have already been studied [11,38], results on the nonequilibrium FDT violation so far are restricted to the spin autocorrelation and response functions [26,27]. In Sec. II A, we introduce the more general class of spin and defect observables we investigate. We briefly present the main result of our method to derive multispin two-time correlation and response functions, as developed in Ref. [39], and summarize the approach used to extract from this the quantities of interest here. Our results for spin dynamical functions are then given in Sec. II B—a preliminary account of which has appeared Ref. [41]—and for defect functions in Sec. II C. In Sec. II D, we discuss the physical aspects of our results for the $1d$ Ising model.

A. General strategy for the calculations

We consider the following spin and defect observables $O_{\rm s}$ and $O_{\rm d}$:

$$O_{\rm s}=\sum_i \epsilon_i s_i \quad \text{and} \quad O_{\rm d}=\sum_i \epsilon_i s_i s_{i+1}. \tag{10}$$

In both cases, ϵ_i are quenched random variables with zero mean $[\epsilon_i]=0$ and translation invariant covariances $q_{i-j}=[\epsilon_i\epsilon_j]$; here $[\cdot]$ denotes the average over the distribution of ϵ. Without loss of generality, we set $q_0=1$. We define the corresponding connected two-time correlation functions

$$C(t,t_{\rm w})=\frac{1}{N}[\langle O_{\rm s}(t)O_{\rm s}(t_{\rm w})\rangle]$$

and

$$C(t,t_{\rm w})=\frac{1}{N}[\langle O_{\rm d}(t)O_{\rm d}(t_{\rm w})\rangle-\langle O_{\rm d}(t)\rangle\langle O_{\rm d}(t_{\rm w})\rangle], \tag{11}$$

for spins and defects, respectively, and the responses

$$R(t,t_{\rm w})=\frac{T}{N}\left[\frac{\delta\langle O_{\rm s}(t)\rangle}{\delta h_{\rm s}(t_{\rm w})}\right]\Bigg|_{h_{\rm s}=0}$$

and

$$R(t,t_{\rm w})=\frac{T}{N}\left[\frac{\delta\langle O_{\rm d}(t)\rangle}{\delta h_{\rm d}(t_{\rm w})}\right]\Bigg|_{h_{\rm d}=0}, \tag{12}$$

where $h_{\rm s}$ and $h_{\rm d}$ are thermodynamically conjugate to $O_{\rm s}$ and $O_{\rm d}$, respectively. All functions are scaled by N to get quantities of the order of unity. It is easy to show that, in the thermodynamic limit $N\to\infty$, Eqs. (11) and (12) become [39]

$$C(t,t_{\rm w})=\sum_n q_n C_n(t,t_{\rm w}) \quad \text{and} \quad R(t,t_{\rm w})=\sum_n q_n R_n(t,t_{\rm w}). \tag{13}$$

Here we have used translational invariance (which holds for our quench from an equilibrium state) to define the distance-dependent correlation functions

$$C_{j-i}(t,t_{\rm w})=\langle s_i(t)s_j(t_{\rm w})\rangle \quad \text{(spins)},$$

$$C_{j-i}(t,t_{\rm w})=\langle s_i(t)s_{i+1}(t)s_j(t_{\rm w})s_{j+1}(t_{\rm w})\rangle-\langle s_i(t)s_{i+1}(t)\rangle \times\langle s_j(t_{\rm w})s_{j+1}(t_{\rm w})\rangle \quad \text{(defects)}, \tag{14}$$

and associated responses

$$R_{j-i}(t,t_{\rm w})=T\left.\frac{\delta\langle s_i(t)\rangle}{\delta h_j(t_{\rm w})}\right|_{h_j=0} \quad \text{(spins)}$$

and

$$R_{j-i}(t,t_{\rm w})=T\left.\frac{\delta\langle s_i(t)s_{i+1}(t)\rangle}{\delta h_{j,j+1}(t_{\rm w})}\right|_{h_{j,j+1}=0} \quad \text{(defects)}. \tag{15}$$

As usual, h_j and $h_{j,j+1}$ are conjugate to s_j and $s_j s_{j+1}$, respectively. Translation invariance also shows that in the thermodynamic limit $N\to\infty$, expressions (11) and (12) are self-averaging, i.e., independent of the particular realization of the disorder variables ϵ_i.

Analysis of the nonequilibrium FDR for the observables $O_{\rm s},O_{\rm d}$ thus requires knowledge of all spin and defect correlation and response functions (14) and (15). We have tackled this problem in Ref. [39] where we give closed, exact solutions for generic two-time multispin correlation and response functions in the Glauber-Ising chain after a quench from an arbitrary equilibrium state at temperature $T_{\rm i}>0$ to any $T\geqslant 0$. The approach is based on the hierarchy of differential equations [40] for the spin correlations $\langle s_{i_1}(t)s_{i_2}(t)\cdots s_{i_k}(t)\rangle$, which we managed to solve *explicitly* for arbitrary initial conditions $\langle s_{i_1}(0)\cdots s_{i_k}(0)\rangle$. Broadly, our technique is to first solve the different levels of the hierarchy separately; each level corresponds to the correlation functions of a given order. The links to lower levels are then incorporated as inhomogeneities. The details are beyond the scope of the present paper but can be found in Ref. [39]; the key result reads

$$\langle s_{i_1}(t)\cdots s_{i_k}(t)\rangle=\sum_{l=0}^{\lfloor k/2\rfloor}\sum_{\pi\in\mathcal{P}(l,k)}(-1)^{\pi}\times\prod_{\lambda=1}^{l}H_{i_{\pi(2\lambda)}-i_{\pi(2\lambda-1)}}(2t)\times\Phi^{(k-2l)}_{(i_{\pi(2l+1)},\ldots,i_{\pi(k)})}(t), \tag{16}$$

$$\Phi^{(k)}_{\boldsymbol{i}}(t)=\sum_{j_1<\cdots j_k}\left(\sum_{\pi\in\mathcal{S}(k)}(-1)^{\pi}\prod_{\lambda=1}^{k}e^{-t}I_{i_\lambda-j_{\pi(\lambda)}}(\gamma t)\right)\times\langle s_{j_1}(0)\cdots s_{j_k}(0)\rangle. \tag{17}$$

Here π denotes permutations and $(-1)^{\pi}$ their sign; $\mathcal{S}(k)$ is the set of all permutations of $\{1,2,\ldots,k\}$ while $\mathcal{P}(l,k)$ is the set of permutations corresponding to choosing l ordered pairs from the numbers $1,2,\ldots,k$ and keeping the remaining $k-2l$ numbers in ascending order. Explicit expressions for the functions $I_n(x)$ and $H_n(x)$ are given in Ref. [39] [for $N\to\infty$ the $I_n(x)$ are the modified Bessel functions, see Appendix A]. We also show in Ref. [39] that the evolution of two-time multispin correlation and response functions is governed by an identical hierarchy of differential equations, so that these quantities can be obtained from Eqs. (16) and (17) if we substitute the corresponding equal-time initial conditions in Eq. (17). The latter are just equal-time correlations—or can be expressed in terms of these for the response functions by generalizing the method developed in Ref. [26]—which we know already. For a quench from an equilibrium state, this leads to explicit results for the two-time multispin functions. As simple examples, we state in Ref. [39] the spin and defect functions (14) and (15) for the quench from $T_{\rm i}=\infty$ to $T\to 0$ considered here. For spins, one finds

$$C_n(t,t_{\rm w})=e^{-(t+t_{\rm w})}\left\{I_n(t+t_{\rm w})+\int_0^{2t_{\rm w}}d\tau\, I_n(t+t_{\rm w}-\tau)\times[I_0+I_1](\tau)\right\}, \tag{18}$$

$$\chi_n(t,t_{\rm w})=\tfrac{1}{2}e^{-t}\int_{t_{\rm w}}^{t}d\tau\, e^{-\tau}I_n(t-\tau)[I_0+2I_1+I_2](2\tau), \tag{19}$$

and for defects

$$C_n(t,t_{\rm w})=\tfrac{1}{2}e^{-(t+t_{\rm w})}[I_{n-1}-I_{n+1}](t+t_{\rm w})\int_{t-t_{\rm w}}^{t+t_{\rm w}}d\tau e^{-\tau}[I_{n-1}-I_{n+1}](\tau)+e^{-2t}\{I_n(t-t_{\rm w})[I_{n-1}+2I_n+I_{n+1}](t+t_{\rm w})-e^{-2t_{\rm w}}[(I_{n-1}+I_n)(I_n+I_{n+1})](t+t_{\rm w})\}, \tag{20}$$

$$\chi_n(t,t_{\rm w})=e^{-2t}\{2\delta_{n,0}[I_0+I_1](2t)-I_n(t-t_{\rm w})[I_{n-1}+2I_n+I_{n+1}](t+t_{\rm w})\}. \tag{21}$$

Here and below the shorthand $[\ldots](x)$ is used to indicate that all functions enclosed in the square brackets have the same argument x; $\delta_{n,0}$ is the standard Kronecker delta. Expressions (19) and (21) for the susceptibilities are more convenient than those for the responses $R_n(t,t_{\rm w})=-(\partial/\partial t_{\rm w})\chi_n(t,t_{\rm w})$ and so we mostly base the following discussion on them. We note that while Eqs. (18) and (19) have already been given in various forms, e.g., Ref. [26], we

are not aware of any equivalent in the literature of Eqs. (20) and (21). The results for the spin response functions given in Ref. [27] differ from ours because these authors used Glauber's original prescription for the spin flip rates [37]; at long times and low T the results become equivalent, however.

Equations (18)–(21) will form the basis for our analysis of the FDR in the $1d$ Ising chain in Secs. II B and II C. For now we return to the observables O_s, O_d and, in particular, the choice of the field covariances q_n. According to Eq. (13), we obtain spin and defect autocorrelation and response functions by choosing uncorrelated random fields ϵ_i, i.e., $q_n = \delta_{n,0}$. We abbreviate the notation in this case to that used in the Introduction and write $C_s(t,t_w)$ for spin and $C_d(t,t_w)$ for defect autocorrelations and similarly $\chi_s(t,t_w)$, $\chi_d(t,t_w)$ for susceptibilities. Uniform covariances $q_n=1$, on the other hand, yield full summations over all cross-correlation and response functions in Eq. (13). So O_s and O_d produce just the magnetization and energy, respectively; we thus use the obvious shorthands $C_m(t,t_w)$, $\chi_m(t,t_w)$, and $C_e(t,t_w)$, $\chi_e(t,t_w)$ for this case. It will turn out that the local ($q_n = \delta_{n,0}$) and global ($q_n=1$) FDT relations for spin and defect observables are very different. Therefore we also investigate intermediate choices of q_n that interpolate between these two extremes. Two classes of covariances can be distinguished. We may interpolate between $q_n=\delta_{n,0}$ and $q_n=1$ by a family of covariances that satisfies $\Sigma_n|q_n|<\infty$ for any nonuniform choice of q_n; we call the corresponding fields ϵ_i short-range correlated. Alternatively, we can interpolate such that $\Sigma_n|q_n|=\infty$ as long as the fields are not completely uncorrelated; we refer to such fields as infinite-range correlated. In either case, the analysis of the FDR for the correlation and response functions of the associated observable requires us to evaluate the infinite sums in Eq. (13). This can be done conveniently in terms of the Fourier transforms $q(k)=\mathcal{F}\{q_n\}$, $C(k;t,t_w)=\mathcal{F}\{C_n(t,t_w)\}$, and $\chi(k;t,t_w)=\mathcal{F}\{\chi_n(t,t_w)\}$, where

$$\mathcal{F}\{f_n\}=\sum_n f_n e^{-ink} \quad \text{and} \quad \mathcal{F}^{-1}\{f(k)\}=\int_{-\pi}^{\pi}\frac{dk}{2\pi}f(k)e^{ink}. \tag{22}$$

In Appendix B, we state the Fourier transforms of Eqs. (18)–(21), in terms of which Eq. (13) becomes

$$C(t,t_w)=\int_{-\pi}^{\pi}\frac{dk}{2\pi}q(k)C(k;t,t_w)$$

and

$$\chi(t,t_w)=\int_{-\pi}^{\pi}\frac{dk}{2\pi}q(k)\chi(k;t,t_w). \tag{23}$$

An explicit example of a family of short-range correlated fields, parametrized by $a>0$, is given by the Lorentzian covariances

$$q_{L,n}=\frac{a^2}{a^2+n^2}\Leftrightarrow q_L(k)=\frac{a\pi}{\sinh a\pi}\cosh a(\pi-|k|). \tag{24}$$

Transform (24) can be found in any table of the Fourier transforms. Equation (24) indeed defines short-range correlated fields: since $q_{L,n}>0$ the criterion becomes $N_c \equiv \Sigma_n q_{L,n}<\infty$ which is satisfied since $N_c=q_L(0) = a\pi\coth a\pi$. By varying a we can also smoothly tune our observables between local ($q_{L,n}\to\delta_{n,0}$ as $a\to 0$) and global ($q_{L,n}\to 1$ for $a\to\infty$) ones. We denote the corresponding correlations and susceptibilities by $C_L(t,t_w)$ and $\chi_L(t,t_w)$. An example of covariances that yield infinite-range correlated fields is

$$q_{P,n}=(-1)^n\frac{\Gamma^2\left(\frac{1+\alpha}{2}\right)}{\Gamma\left(\frac{1+\alpha}{2}-n\right)\Gamma\left(\frac{1+\alpha}{2}+n\right)}$$

$$\Leftrightarrow q_P(k)=\frac{\Gamma^2\left(\frac{1+\alpha}{2}\right)}{2^{1-\alpha}\Gamma(\alpha)}\left|\sin\frac{k}{2}\right|^{\alpha-1}, \tag{25}$$

where $0<\alpha<1$ and $\Gamma(x)$ is the Gamma function [42]. It is clear from Eq. (25) that $q_{P,n}$ is even in n and $q_{P,0}=1$. We show in Appendix C that for $\alpha\to 1$ we get $q_{P,n}=\delta_{n,0}$ while $\alpha\to 0$ gives $q_{P,n}=1$. We also prove there that $q_{P,n}$ decreases monotonically as $|n|$ increases, decaying asymptotically as a power law $q_{P,n}\sim|n|^{-\alpha}$, and that indeed $\mathcal{F}^{-1}\{q_P(k)\} = q_{P,n}$. The reverse transform $\mathcal{F}\{q_{P,n}\}$ does not converge in the usual sense, but this is not necessary for the equivalence of Eqs. (13) and (23). So Eq. (25) again allows us to interpolate smoothly between local and global observables, but in such a way that $\Sigma_n q_{P,n}=\infty$ for any $\alpha\in[0,1[$. The correlations and susceptibilities for the observables defined by fields ϵ_i with the power-law covariances (25) are denoted by $C_P(t,t_w)$ and $\chi_P(t,t_w)$ below.

B. Spin observables

1. Random field: Incoherent functions

The FDT violation for the spin autocorrelation and response functions has already been studied in detail in Refs. [26,27]. In particular, it was shown that the FD plot approaches a nontrivial limit curve in the aging regime, with $X_s^\infty=\frac{1}{2}$. We can easily recover the existing results for $C_s(t,t_w),\chi_s(t,t_w)$ from our exact solutions (18) and (19) by setting $n=0$. It is useful to focus on the aging limit. Formally, this is an asymptotic expansion in the limit $t,t_w\to\infty$ with $\epsilon\leqslant t_w/t\leqslant 1-\delta$ fixed and $\epsilon,\delta>0$, to ensure that t,t_w, and Δt all diverge and are of the same order. In this limit, the asymptotic expansion (A3) for the modified Bessel functions yields immediately

$$C_s(t,t_w)\sim\frac{2}{\pi}\arcsin\sqrt{\frac{2t_w}{t+t_w}}, \tag{26}$$

$$\chi_s(t,t_w)\sim\frac{\sqrt{2}}{\pi}\arccos\sqrt{\frac{t_w}{t}}. \tag{27}$$

Here and below, the "$\sim$" sign denotes results which are asymptotically exact in the aging limit. The limit FD plot corresponding to Eqs. (26) and (27) is contained in Fig. 2 below and the associated FDR is a function of the time ratio t_w/t only,

$$X_s(t,t_w) \sim \frac{t+t_w}{2t}. \tag{28}$$

It shows a continuous crossover from $X_s(t,t_w)=1$ for $\Delta t \ll t_w$ to $X_s(t,t_w)=X_s^\infty=\frac{1}{2}$ for $\Delta t \gg t_w$. We note that the aging expansion of the spin correlations and susceptibilities (18) and (19) is dominated by the leading term of the asymptotic series (A3) for the modified Bessel functions, which is independent of the order n. Therefore, Eqs. (26) and (27) in fact apply to all finite-distance spin cross correlations and susceptibilities $C_n(t,t_w)$, $\chi_n(t,t_w)$. Consequently, the latter produce the same limiting FD plot and FDR (28) as for $n=0$.

2. Uniform field: Coherent functions

As described, the uniform field effectively allows us to study the FDR for the magnetization. The corresponding correlation and susceptibility are most conveniently obtained from the Fourier transforms (B1) and (B2) by setting $k=0$; the time integrals appearing in $C(k;t,t_w)$, $\chi(k;t,t_w)$ can then be solved. One finds

$$C_m(t,t_w)=e^{-2t_w}\{I_0(2t_w)+4t_w[I_0+I_1](2t_w)\}, \tag{29}$$

$$R_m(t,t_w)=\tfrac{1}{2}e^{-2t_w}[I_0+2I_1+I_2](2t_w). \tag{30}$$

We have given the response $R=-\partial\chi/\partial t_w$ here rather than the susceptibility because it has a simpler form. Note that both the correlation and response functions (29) and (30) are independent of t. This can be understood from the fact that for $T=0$ the magnetization $m=(1/N)\Sigma_i s_i$ performs a random walk with step size $\pm 2/N$ and a time-dependent rate $\frac{1}{2}Nc$, where c is the concentration of domain walls. The latter can be obtained explicitly from Eq. (18) by setting $t=t_w$ and $n=1$, since $C_1(t_w,t_w)=\langle s_i(t_w)s_{i+1}(t_w)\rangle=1-2c(t_w)$. This gives [43]

$$c(t_w)=\tfrac{1}{2}e^{-2t_w}[I_0+I_1](2t_w). \tag{31}$$

Now, since the random walk of m is unbiased, $C_m(t,t_w)=N\langle m(t)m(t_w)\rangle=C_m(t_w,t_w)$ follows immediately. Also, $C_m(t_w,t_w)$ will grow with rate $2ND(t_w)$, where $D=(2/N)^2\frac{1}{2}Nc=2c/N$ is the diffusion constant. One should thus have $\partial C_m(t_w,t_w)/\partial t_w=4c(t_w)$, and from Eqs. (29) and (31) one verifies that this is indeed the case. Similar arguments apply to the response $R_m(t,t_w)$. Brief application of a field at t_w biases the domain-wall motion and hence the random walk of m; thereafter the random walk is again unbiased and so the response must be t independent. The momentary bias in the random-walk rates contains the domain-wall concentration $c(t_w)$ as an overall factor, and consistent with this expectation one gets $R_m(t,t_w)\sim 2c(t_w)$ asymptotically.

Since both $C_m(t,t_w)$ and $R_m(t,t_w)$ are functions of t_w only, this also applies to the FDR

$$X_m(t_w)=\frac{[I_0+2I_1+I_2](2t_w)}{4[I_0+I_1](2t_w)}, \tag{32}$$

which crosses over from the initial value $X_m(0)=\frac{1}{4}$ to $\frac{1}{2}$ on an $O(1)$ time scale. So, apart from a transient after the quench, we measure $X_m(t_w)=\frac{1}{2}$ for all $t \gtrsim t_w \gg 1$; in particular, the limiting value $X_m(t_w)\sim X_m^\infty=X_s^\infty=1/2$ in the aging regime is identical to that for the incoherent spin observables. Note that there is no quasiequilibrium regime with $X_m=1$ for $\Delta t \ll t_w$. The corresponding FD plot converges to a straight line of slope $\frac{1}{2}$ (see Fig. 2 below).

3. Short-range correlated field

Next we investigate the effect of short-range correlations in the random fields ϵ_i on the FDR. The correlations and susceptibilities of the corresponding observables may be obtained either from a real-space summation (13) or an integration in the Fourier representation (23). Using the latter, we note first that the short-range criterion $\Sigma_n|q_n|<\infty$ for the covariances implies that $q(k)=\mathcal{F}\{q_n\}=\Sigma_n q_n e^{-ink}$ is a continuous function. The Fourier transforms $C(k;t,t_w)$, $\chi(k;t,t_w)$, on the other hand, satisfy

$$\frac{C(k;t,t_w)}{C_s(t,t_w)} \to 2\pi\tilde{\delta}(k) \quad \text{and} \quad \frac{\chi(k;t,t_w)}{\chi_s(t,t_w)} \to 2\pi\tilde{\delta}(k) \tag{33}$$

in the aging limit, where $\tilde{\delta}(\cdot)$ is a 2π-periodic version of the ordinary Dirac delta. The normalizations of the right-hand sides of Eq. (33) are clear, since $C_s(t,t_w)$, for instance, is given by the Fourier integral (22) over $C(k;t,t_w)$ for $n=0$. Also, since $C_s(t,t_w)$ and $\chi_s(t,t_w)$ are $\mathcal{O}(1)$ functions of t_w/t in the aging limit, while $C(k;t,t_w)$, $\chi(k;t,t_w)$ vanish in the same limit for any k that is not a multiple of 2π, Eq. (33) follows. This in turn implies that for any short-range correlated field,

$$C(t,t_w)\sim N_c C_s(t,t_w) \quad \text{and} \quad \chi(t,t_w)\sim N_c\chi_s(t,t_w) \tag{34}$$

provided that $N_c=q(0)=\Sigma_n q_n$, which estimates the number of lattice sites over which field correlations extend, is nonzero. So in the aging limit, the correlations and susceptibilities are ultimately just proportional to Eqs. (26) and (27) and hence yield the same FDR and FD plot as the local spin functions. This statement can equivalently be made in real space, based on the convergence of the series q_n and the fact that all finite-distance cross-correlation and response functions behave asymptotically as Eqs. (26) and (27).

At finite times, however, we find a crossover between two dynamical regimes. A scaling analysis shows that the peaks in $C(k;t,t_w)$ and $\chi(k;t,t_w)$ at $k=0$ have widths $t^{-1/2}$ and $\Delta t^{-1/2}$, respectively. Correspondingly, we have growing length scales in real space. These are $\ell_C \approx t^{1/2}$ for correlations, corresponding to the typical domain size, but $\ell_\chi \approx \Delta t^{1/2}$ for the response which reflects the fact that perturba-

tions spread diffusively. When $\ell_C, \ell_\chi \gg N_c$, one has an effectively local observable and we are in the asymptotic regime (34). If, however, $\ell_C, \ell_\chi \ll N_c$, the fields ϵ_i are correlated over distances much longer than the dynamical length scales, giving an effectively uniform field. One thus expects to get an FD plot similar to that obtained for the magnetization. The illustration of the crossover in Fig. 1, obtained by numerical integration of Eq. (23), shows that this is indeed the case.

4. Infinite-range correlated field

For infinite-range correlated fields, one cannot use simple scaling arguments, since the correlations and susceptibilities contain contributions from all length scales. For the power-law covariances (25) introduced above, this is reflected in the singularity of $q_P(k)$ at $k=0$. Therefore we have to analyze the full expressions for $C_P(t,t_w)$ and $\chi_P(t,t_w)$ that follow from Eq. (23) after substitution of $q_P(k)$, $C(k;t,t_w)$, and $\chi(k;t,t_w)$. Fortunately, for the particular choice of $q_P(k)$ the results may be expressed in terms of single integrals of the form

$$C_P(t,t_w) = e^{-2(t+t_w)}\Bigg\{ {}_1F_1\left(\frac{1}{2},\frac{1+\alpha}{2};2(t+t_w)\right) + \int_0^{2t_w} d\tau e^{\tau}\, {}_1F_1\left(\frac{1}{2},\frac{1+\alpha}{2};2(t+t_w-\tau)\right) \times [I_0+I_1](\tau)\Bigg\}, \tag{35}$$

$$\chi_P(t,t_w) = \frac{1}{2}e^{-2t}\int_{t_w}^{t} d\tau\, {}_1F_1\left(\frac{1}{2},\frac{1+\alpha}{2};2(t-\tau)\right) \times [I_0+2I_1+I_2](2\tau), \tag{36}$$

where ${}_1F_1(\alpha,\gamma;z)$ is the confluent hypergeometric function [42]. Equations (35) and (36) are exact and can be used to study the FD plots and the FDR numerically. However, in the aging limit, asymptotic expansions may be substituted for the nonelementary functions and significant simplifications are possible. One finds

$$C_P(t,t_w) \sim \frac{2^{(1-\alpha)/2}}{\pi}\Gamma\left(\frac{1+\alpha}{2}\right)(t+t_w)^{(1-\alpha)/2} \times B\left(\frac{1}{2},1-\frac{\alpha}{2};\frac{2t_w}{t+t_w}\right), \tag{37}$$

$$\chi_P(t,t_w) \sim \frac{2^{-\alpha/2}}{\pi}\Gamma\left(\frac{1+\alpha}{2}\right)t^{(1-\alpha)/2}\left[B\left(\frac{1}{2},1-\frac{\alpha}{2}\right) - B\left(\frac{1}{2},1-\frac{\alpha}{2};\frac{t_w}{t}\right)\right], \tag{38}$$

where $B(p,q;x)$ is the incomplete beta function $B(p,q;x) = \int_0^x du\, u^{p-1}(1-u)^{q-1}$ and $B(p,q)=B(p,q;1)$ is the complete one [42]. In the random-field limit, $\alpha \to 1$, we recover expansions (26) and (27) for the incoherent functions since $B(\frac{1}{2},\frac{1}{2};x) = 2\arcsin\sqrt{x}$, whereas the uniform field limit α

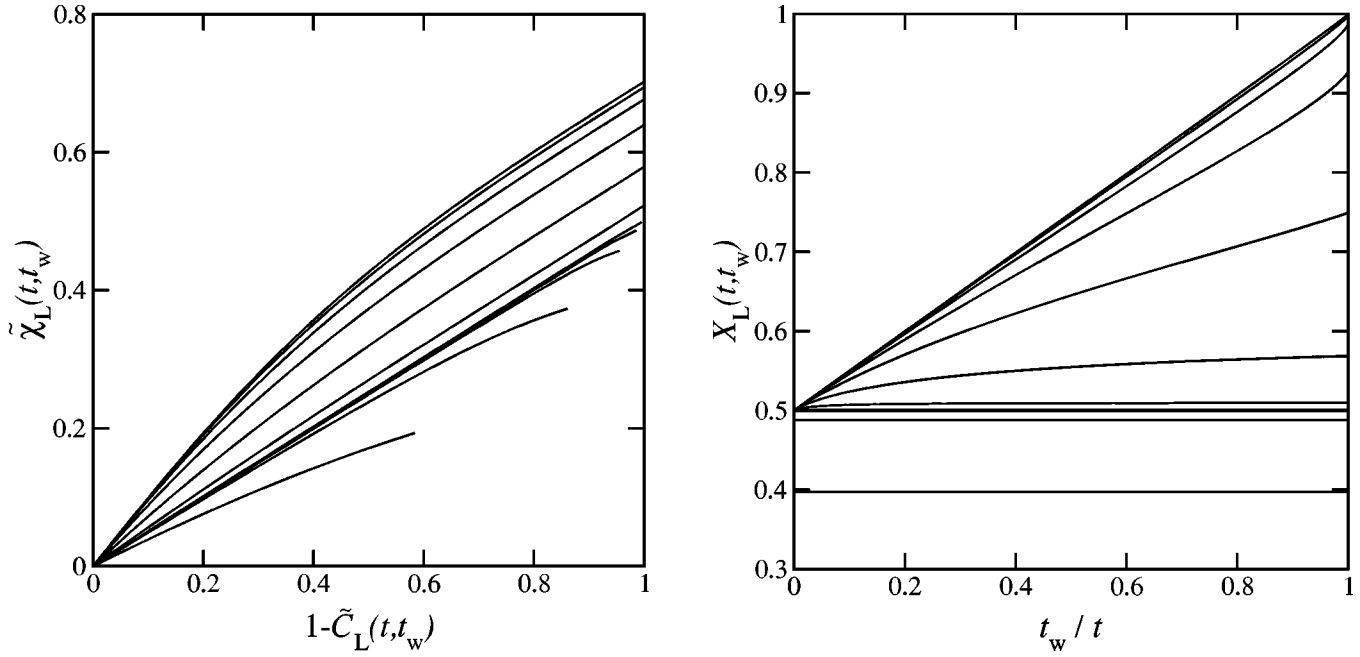

FIG. 1. Normalized FD plot (left) and the corresponding FDR vs t_w/t (right) for a random field with Lorentzian covariances (24) with $a=10^3$, correlated over $N_c = a\pi \coth a\pi \approx a\pi$ sites. In the FD plot, t is fixed for each curve and varies over the range $10^0, 10^1, \ldots, 10^{10}$ (bottom to top). The lines first converge towards the straight line with slope $\frac{1}{2}$ corresponding to a coherent observable (the magnetization) but eventually, for $t \geqslant 10^5$, cross over to the limit plot for uncorrelated fields. This behavior is also reflected in the evolution of $X_L(t,t_w)$. There, however, we have the freedom to fix either t or t_w. The plot shows the case of fixed t_w, which is more convenient for comparison with simulations, for $t_w = 10^0, \ldots, 10^{10}$ (bottom to top).

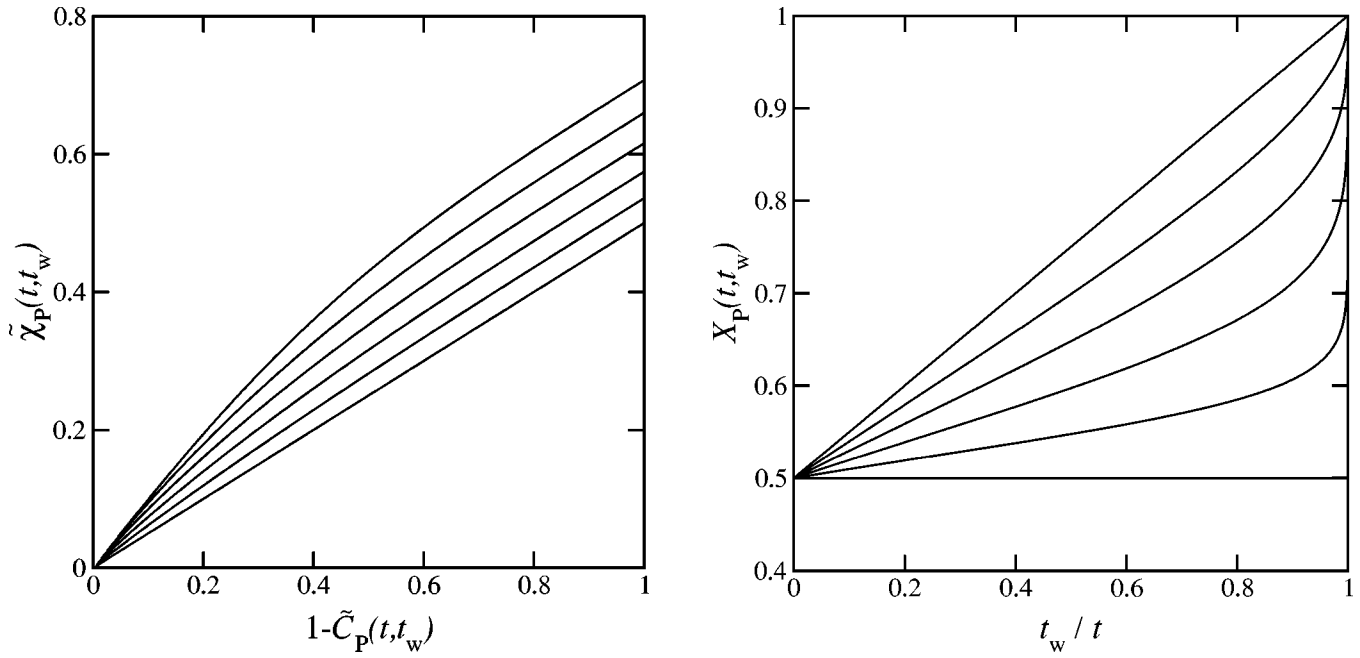

FIG. 2. Normalized FD plots (left) and the corresponding FDR vs t_w/t (right) in the aging limit $t,t_w\to\infty$. The bottom curves in both plots are for the magnetization (Sec. II B 2) and coincide with the uniform field limit $\alpha\to 0$ of the power-law field covariances. The intermediate curves are for power laws (Sec. II B 4) with exponents $\alpha=0.2,0.4,0.6,0.8$ (bottom to top). The top curves represent the random-field limit $\alpha\to 1$ for power laws, and apply also to any short-range correlated field (Sec. II B 3) with $N_c\neq 0$ or, in the extreme case, the incoherent functions of Sec. II B 1.

$\to 0$ can be shown to coincide, using $B(\frac{1}{2},1;x)=2\sqrt{x}$, with the asymptotic expansions of Eqs. (29) and (30) for the coherent functions. So the power-law covariances (25) indeed allow us to interpolate between the coherent and incoherent observables. For intermediate exponents $0<\alpha<1$, the fluctuations in the observable O_s grow as $t_w^{(1-\alpha)/2}$ and the two-time correlation (37) has a plateau at a corresponding value for $\Delta t\ll t_w$; for $\Delta t\gg t_w$ it decays as $t_w^{(1-\alpha)/2}(t_w/\Delta t)^{\alpha/2}$. For the susceptibility, we deduce from Eq. (38) a $\Delta t^{(1-\alpha)/2}(\Delta t/t_w)^{1/2}$ growth for $\Delta t\ll t_w$ that crosses over to $\Delta t^{(1-\alpha)/2}$ for $\Delta t\gg t_w$. Figure 2 shows exact FD limit plots that follow from Eqs. (37) and (38). The associated FDR may be obtained from Eqs. (37) and (38) as

$$X_P(t,t_w)\sim\left\{\frac{2t}{t+t_w}+\frac{1-\alpha}{2}\sqrt{\frac{2t_w}{t+t_w}}\left(\frac{t-t_w}{t+t_w}\right)^{\alpha/2}\times B\left(\frac{1}{2},1-\frac{\alpha}{2};\frac{2t_w}{t+t_w}\right)\right\}^{-1}. \tag{39}$$

In principle, one should first differentiate Eqs. (35), (36) to obtain $R_P(t,t_w)$ and $(\partial/\partial t_w)C_P(t,t_w)$ and then perform the aging expansion, but this turns out to give the same result. Equation (39) is a function of t_w/t only and interpolates between the FDR (28) for the local spin observables ($\alpha\to 1$) and the constant $X_m^\infty=\frac{1}{2}$ for the magnetization ($\alpha\to 0$). Plots of $X_P(t,t_w)$ for various powers α are also shown in Fig. 2. It is remarkable that the FDR again crosses over from $X_P(t,t_w)=1$ for $\Delta t\ll t_w$ to $X_P^\infty=\frac{1}{2}$ for $\Delta t\gg t_w$, independently of the power-law exponent α.

5. Harmonically correlated fields and X^∞

The explicit examples given in Secs. II B 1–II B 4 suggest that $X^\infty=\frac{1}{2}$ is a generic feature for the spin observables O_s defined in Eq. (10). To show that this is indeed true, we start from the fact that for a general observable O_s the correlation and susceptibility—and hence $(\partial/\partial t_w)C(t,t_w)$ and $R(t,t_w)$—may be written in form (23). By introducing a generalized FDT for the Fourier modes,

$$R(k;t,t_w)=X(k;t,t_w)\frac{\partial}{\partial t_w}C(k;t,t_w), \tag{40}$$

we may express $R(k;t,t_w)$ via Eq. (40) and thereby obtain the following representation for the FDR $X(t,t_w)$ associated with a generic spin observable O_s:

$$X(t,t_w)=\frac{\int_{-\pi}^{\pi}\frac{dk}{2\pi}X(k;t,t_w)q(k)\frac{\partial}{\partial t_w}C(k;t,t_w)}{\int_{-\pi}^{\pi}\frac{dk}{2\pi}q(k)\frac{\partial}{\partial t_w}C(k;t,t_w)}. \tag{41}$$

This means that $X(t,t_w)$ may be considered as the average of $X(k;t,t_w)$ over the normalized distribution of $q(k)(\partial/\partial t_w)C(k;t,t_w)$ on $k\in[-\pi,\pi]$. The FDR for Fourier modes follows from Eq. (40) and expressions (B1) and (B2) for $C(k;t,t_w),\chi(k;t,t_w)$ as

$$X(k;t_w)=\frac{[I_0+2I_1+I_2](2t_w)}{4[I_0+I_1](2t_w)-2(1-\cos k)\left\{e^{2t_w\cos k}+\int_0^{2t_w}d\tau e^{(2t_w-\tau)\cos k}[I_0+I_1](\tau)\right\}}, \tag{42}$$

and is a function of t_w and k only. For $k=0$, Eq. (42) reduces to the FDR for the magnetization $X_m(t_w)$ (32) and hence $X(0;t_w)\approx\frac{1}{2}$ for $t_w\gg 1$. A scaling analysis of Eq. (42) shows that for $|k|\ll\pi$ and $t_w\gg 1$ we get $X(k;t_w)\approx X(k^2t_w)$ with $X(k^2t_w)\approx\frac{1}{2}$ for $k^2t_w\ll 1$ and $X(k^2t_w)\approx 1$ when $k^2t_w\gg 1$. So Eq. (42) reflects the successive equilibration of increasing length scales.

Now we can return to the FDR (41) for the observable O_s. For the magnetization—being the coherent observable—we have $q(k)=2\pi\tilde{\delta}(k)$ and Eq. (41) reduces to the trivial identity $X_m(t_w)=X(0;t_w)$. In physical terms, by selecting the coherent observable we only measure the FDR associated with the infinite length scale. For other spin observables, being characterized by the function $q(k)$, the FDR $X(t,t_w)$ contains contributions from all length scales. For the long-time limit X^∞, however, the situation simplifies because $(\partial/\partial t_w)C(k;t,t_w)$ develops an infinitely sharp peak at $k=0$ as $t\to\infty$. This can be verified by a scaling analysis of Eq. (B1). For sufficiently well-behaved functions $q(k)$, the normalized version of the distribution $q(k)(\partial/\partial t_w)C(k;t,t_w)$ thus becomes a realization of $\tilde{\delta}(k)$ and we get $X(t,t_w)\to X(0;t_w)$ as $t\to\infty$. Taking the limit $t_w\to\infty$ then shows that $X^\infty=\frac{1}{2}$, as claimed. So for a generic spin observable, X^∞ again just gives the FDR associated with the infinite length scale. The only exception occurs when this contribution is explicitly suppressed. An example of the latter case would be harmonically correlated fields, $q_n=\cos np$ with $0<p<\pi$: for such observables $X(t,t_w)=X(p;t_w)$ and hence $X^\infty=1$.

C. Defect observables

1. Random field: Incoherent functions

The defect observable O_d given in Eq. (10) with random, uncorrelated fields ϵ_i allows us to study the FDT violation for local defect correlations and susceptibilities. These follow from Eqs. (20) and (21) by setting $n=0$, giving

$$C_d(t,t_w)=2e^{-2t}I_0(t-t_w)[I_0+I_1](t+t_w)-e^{-2(t+t_w)}\times[I_0+I_1]^2(t+t_w), \tag{43}$$

$$\chi_d(t,t_w)=2e^{-2t}\{[I_0+I_1](2t)-I_0(t-t_w)[I_0+I_1](t+t_w)\}. \tag{44}$$

These results can be written in a more physically intuitive way in terms of the concentration of domain walls $c(t)$, Eq. (31), and the return probability $p_r(\tau)=e^{-\tau}I_0(\tau)$ of a continuous-time random walker on a discrete, one-dimensional lattice [44]. Expressing all time dependencies in Eq. (43) and (44) via $c(t)$ and $p_r(\tau)$ yields the exact identities

$$C_d(t,t_w)=4c\left(\frac{t+t_w}{2}\right)\left[p_r(t-t_w)-c\left(\frac{t+t_w}{2}\right)\right], \tag{45}$$

$$\chi_d(t,t_w)=4\left[c(t)-p_r(t-t_w)c\left(\frac{t+t_w}{2}\right)\right]. \tag{46}$$

The fact that we find random-walk-related quantities does not come as a surprise given that there is an exact mapping of zero-temperature Glauber dynamics in the Ising chain to a diffusion-limited pair-annihilation (DLPA) process [45]. The mapping follows by assigning to each bond $(i,i+1)$ the "particle" occupation number $b_i=\frac{1}{2}(1-s_is_{i+1})\in\{0,1\}$ which signals the presence or absence of a domain wall. Glauber dynamics for the spins corresponds to independent random walks for the particles and coalescence of domains of aligned spins yields particle pair annihilation.

It follows from definition (14) of the defect autocorrelation that $C_d(t,t_w)=4[\langle b_i(t)b_i(t_w)\rangle-\langle b_i(t)\rangle\langle b_i(t_w)\rangle]$ in fact also describes the particle autocorrelation in the DLPA process. We note that Eq. (45) is a nontrivial result. Assuming as in Ref. [36] that the autocorrelation of the fraction $c(t)$ of particles that still exist at time t is given by $p_r(t-t_w)$ and that these particles are uncorrelated with the fraction $c(t_w)-c(t)$ of particles that have disappeared via annihilation, one would conclude $\langle b_i(t)b_i(t_w)\rangle=c(t)p_r(t-t_w)+c(t)[c(t_w)-c(t)]$ and hence $C_d(t,t_w)=4c(t)[p_r(t-t_w)-c(t)]$. This obviously differs from the exact solution (45). As an approximation it holds for $\Delta t\ll t_w$, but breaks down for $\Delta t\gg t_w$ where Eq. (45) yields $C_d(t,t_w)\approx 2t_w/(\pi\Delta t^2)$ whereas the approximation gives $C_d(t,t_w)\approx(\sqrt{2}-1)/(\pi\Delta t)$. This shows that two-time correlations in $C_d(t,t_w)$ build up via a rather subtle mechanism, the explanation of which in terms of the DLPA would probably require knowledge of the interparticle (i.e., domain size) distribution. Similarly, it appears that result (46) cannot be obtained in a straightforward way.

Now we turn to the dynamics of $C_d(t,t_w)$, $\chi_d(t,t_w)$—examples of which are shown in Fig. 3—as given by Eqs. (45) and (46). The equal-time value of $C_d(t_w,t_w)=4c(t_w)[1-c(t_w)]\approx 4c(t_w)\approx 2/\sqrt{\pi t_w}$ for $t_w\gg 1$ decreases with t_w, reflecting the decreasing number of particles in the DLPA process (or domain walls in the spin chain). In the regime $\Delta t\ll t_w$, the two-time correlation $C_d(t,t_w)\approx 4c(t_w)p_r(\Delta t)$ drops from its initial value due to the random-walk motion of the particles around their initial positions at t_w. In the aging limit of large Δt and t_w, one has the expansion $C_d(t,t_w)\sim 2/(\pi\sqrt{t+t_w})(1/\sqrt{t-t_w}-1/\sqrt{t+t_w})$. This crosses over from $C_d(t,t_w)\approx 2/(\pi\sqrt{2\Delta t t_w})$ for $\Delta t\ll t_w$, where it connects smoothly to the initial drop for Δt of $O(1)$, since $p_r(\Delta t)\approx 1/\sqrt{2\pi\Delta t}$ for

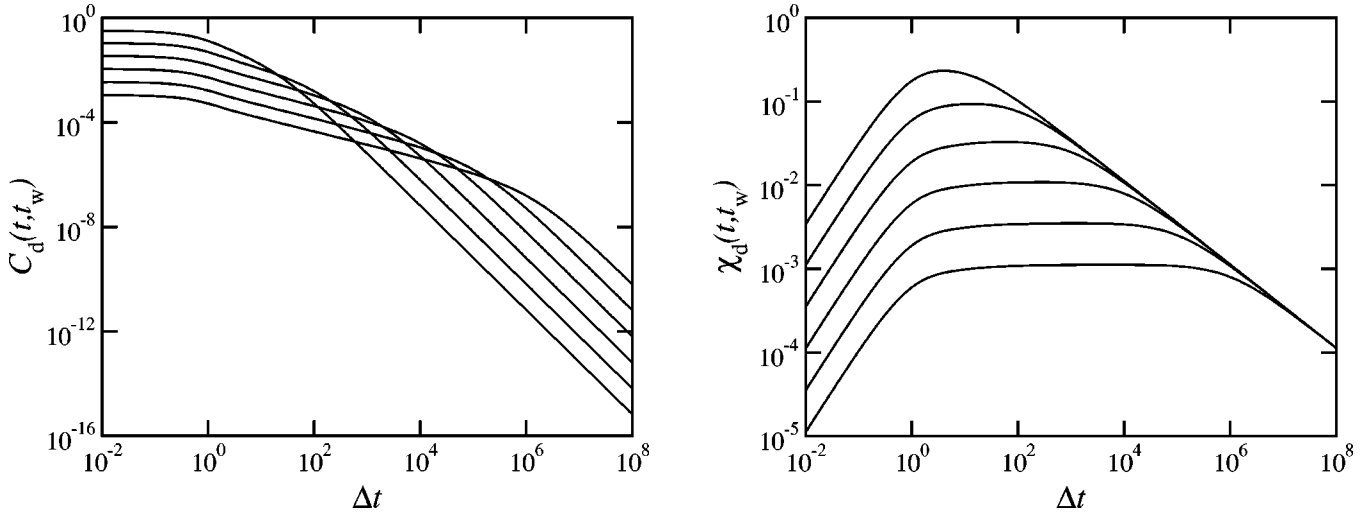

FIG. 3. Defect autocorrelation (left) and susceptibility (right) vs Δt for waiting times $t_w = 10^1, 10^2, \ldots, 10^6$. Increasing waiting times corresponds to decreasing values in the plot for small Δt.

large Δt, to $C_d(t,t_w) \approx 2t_w/(\pi \Delta t^2)$ for $\Delta t \gg t_w$. The integrated response $\chi_d(t,t_w)$ is nonmonotonic in Δt and increases on an $O(1)$ time scale in Δt from its initial value $\chi_d(t_w,t_w)=0$ to a plateau $\chi_d(t,t_w) \approx 2/\sqrt{\pi t_w}$ for $\Delta t \ll t_w$ according to $\chi_d(t,t_w) \approx 4c(t_w)[1-p_r(t-t_w)]$. This crossover is clear from the spin-chain dynamics: the perturbation associated with $\chi_d(t,t_w)$ is $\delta H = -h s_i s_{i+1}$ which simply increases the coupling between sites i, $i+1$. This enforces alignment of the spins s_i and s_{i+1} and hence increases $\langle s_i(t) s_{i+1}(t) \rangle$ on a microscopic time scale. In the aging limit, the leading term in the integrated response is just $\chi_d(t,t_w) \sim 2/\sqrt{\pi t}$ which connects to the plateau $\chi_d(t,t_w) \approx 2/\sqrt{\pi t_w}$ for $\Delta t \ll t_w$ but eventually decreases as $\chi_d(t,t_w) \approx 2/\sqrt{\pi \Delta t}$ for $\Delta t \gg t_w$.

For constructing a FD plot (Fig. 4), we are interested in keeping t fixed and varying t_w between 0 and t; the functions $C_d(t,t_w)$ and $\chi_d(t,t_w)$ are then monotonic in t_w. In fact, the exact expressions (45) and (46) satisfy $C_d(t,t) - C_d(t,t_w) = \chi_d(t,t_w) + 4(c^2[(t+t_w)/2] - c^2(t))$. Dividing this relation by the equal-time value $C_d(t,t)$ yields the relevant normalized quantities

$$1 - \tilde{C}_d(t,t_w) = \tilde{\chi}_d(t,t_w) + \frac{c^2\left(\frac{t+t_w}{2}\right) - c^2(t)}{c(t)[1-c(t)]} = \tilde{\chi}_d(t,t_w) + O\left(\frac{1}{\sqrt{t}} \frac{t-t_w}{t+t_w}\right). \quad (47)$$

In the limit $t \to \infty$ the extra term in Eq. (47) vanishes and we get $1 - \tilde{C}_d(t,t_w) = \tilde{\chi}_d(t,t_w)$ for all $0 \leq t_w/t \leq 1$. This, however, does not imply that the equilibrium FDT holds, i.e., $X_d(t,t_w)=1$. In fact, working out $(\partial/\partial t_w) C_d(t,t_w)$ and $R_d(t,t_w)$ from Eqs. (45) and (46) and expanding their ratio in the aging limit give

$$X_d(t,t_w) \sim \frac{t_w(t+t_w)}{t_w(t+t_w) + (t-t_w)\sqrt{t^2 - t_w^2}}. \quad (48)$$

The FDR (48) is a function of the time ratio t_w/t and crosses over from $X_d(t,t_w)=1$ for $t_w/t \to 1$ to $X_d(t,t_w) = X_d^\infty = 0$ for $t_w/t \to 0$ (Fig. 4). This seemingly paradoxical result can easily be explained in terms of the expansions given above. In the regime $\Delta t \ll t$ (which is equivalent to $\Delta t \ll t_w$, as considered before), we have, up to subleading corrections for $t \to \infty$, $C_d(t,t_w) \approx 4c(t) p_r(t-t_w)$ and $\chi_d(t,t_w) \approx 4c(t)[1 - p_r(t-t_w)]$. So the equilibrium FDT indeed holds in this regime and the DLPA process is, to leading order, just an ensemble of independent random walks. Now recall that $p_r(\Delta t) \approx 1/\sqrt{2\pi \Delta t}$ for $\Delta t \gg 1$. So at the point where this approximation breaks down, $\Delta t \approx t$, the value of, e.g., $C_d(t,t_w)$ decreases to an arbitrary small fraction of $C_d(t,t)$ as t increases. This leads to a straight line segment which eventually covers the whole of the (normalized) FD plot while the size of the nontrivial region shrinks as $1/\sqrt{t}$. In the latter part, for $\tilde{C}_d(t,t_w) \ll 1/\sqrt{\pi t}$, one has from the aging expansions of $C_d(t,t_w)$ and $\chi_d(t,t_w)$,

$$1 - \tilde{\chi}_d(t,t_w) \approx \frac{1}{\sqrt{\pi t}} + \frac{\sqrt{\pi t}}{2} \tilde{C}_d^2(t,t_w). \quad (49)$$

Hence the FD plot indeed turns horizontal as $\tilde{C}_d(t,t_w)$ approaches zero, consistent with Eq. (48). In summary, a FD plot is not the appropriate representation for the FDT violation measured by the defect autocorrelation and response. A plot of the FDR as a function of t_w/t, however, converges to the nontrivial limit curve given by Eq. (48) as times diverge, see Fig. 4.

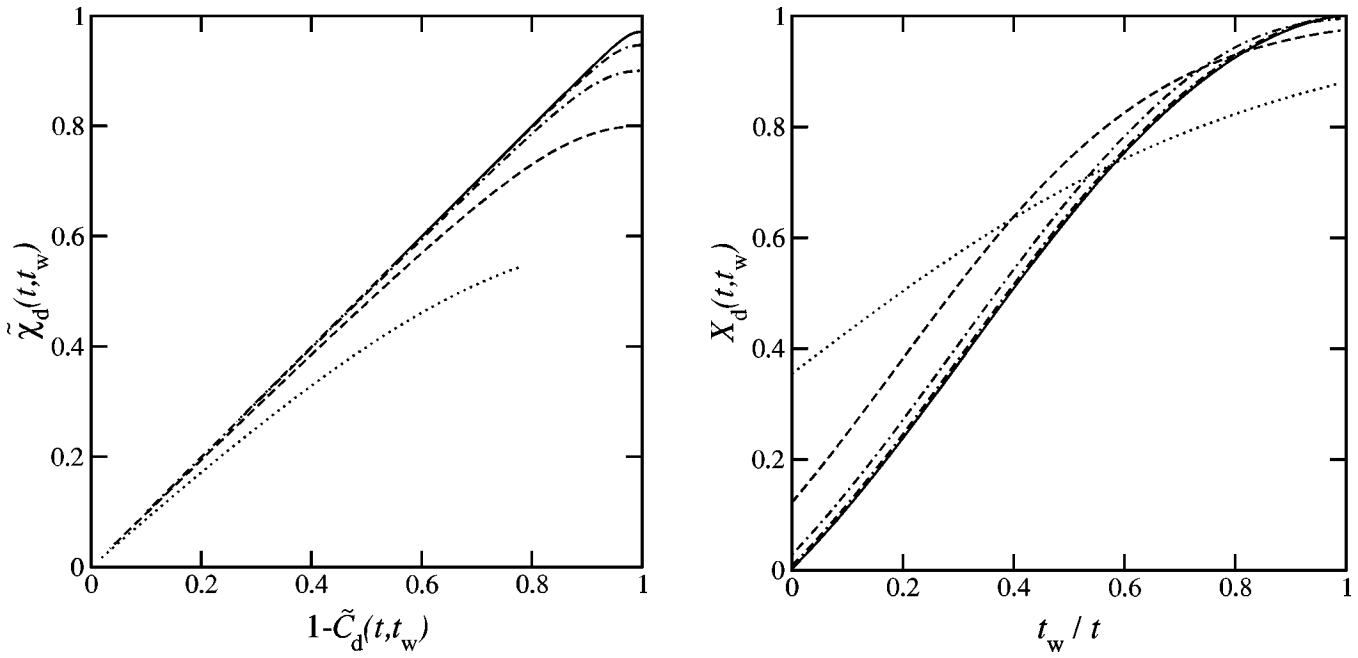

FIG. 4. Normalized FD plot (left) and the corresponding FDR vs t_w/t (right) for the defect autocorrelation and susceptibility. In both plots t is kept fixed, giving a one-to-one correspondence of the curves, and varies over the range $t=10^0$ (dotted), $10^{1/2},10^1,10^{3/2},10^2$ (solid). The curves of $X_d(t,t_w)$ for $t=10^{3/2},10^2$ are almost indistinguishable and very close to the limit curve (48).

2. Uniform field: Coherent functions

For uniform covariances $q_n=1$, the defect observable O_d is equivalent to the total energy of the system. According to Eq. (23) we have $C_e(t,t_w)=C(0;t,t_w)$, which may be simplified to give

$$C_e(t,t_w)=4e^{-2t}[I_0+I_1](2t)-e^{-2(t+t_w)} \times[3I_0+4I_1+I_2](2t+2t_w). \tag{50}$$

This result again has an analog in the associated DLPA process, where it describes the normalized two-time correlation of the total number of particles $\mathcal{N}$, $C_e(t,t_w)=(4/N)[\langle\mathcal{N}(t)\mathcal{N}(t_w)\rangle-\langle\mathcal{N}(t)\rangle\langle\mathcal{N}(t_w)\rangle]$. A result similar to Eq. (50) was given in Ref. [46], for initial conditions corresponding formally to equilibrium at inverse temperature $1/T=-\infty$. Up to a factor of 4 which appears to be missing in Ref. [46], it coincides with Eq. (50) for large t_w, where one finds the simple scaling form $C_e(t,t_w)\sim 4/\sqrt{\pi}(1/\sqrt{t}-1/\sqrt{t+t_w})$. At *equal* times, fluctuations in the energy follow as $C_e(t_w,t_w)\sim(2-\sqrt{2})C_d(t_w,t_w)$. This shows that in $C_e(t_w,t_w)=\Sigma_n C_n(t_w,t_w)$, the nonlocal $(n\neq 0)$ terms make a contribution $-(\sqrt{2}-1)C_d(t_w,t_w)$, of the same order as the local term but with opposite sign. For $\Delta t\ll t_w$, the two-time correlation $C_e(t,t_w)\approx C_e(t_w,t_w)$ has a plateau but it decreases as $C_e(t,t_w)\approx 2t_w/(\Delta t\sqrt{\pi\Delta t})$ when $\Delta t\gg t_w$.

By setting $k=0$ in the Fourier transform (B4) we find that $\chi_e(t,t_w)=\chi(0;t,t_w)\equiv 0$ at all times. This is for the simple reason that the perturbation is proportional to the Hamiltonian and therefore just rescales the temperature, which obviously has no effect in the $T\to 0$ limit considered here. We note that $\chi_e(t,t_w)=\Sigma_n\chi_n(t,t_w)=0$ implies that the sum over all cross susceptibilities $(n\neq 0)$ exactly balances the local susceptibility $\chi_d(t,t_w)\equiv\chi_0(t,t_w)$.

A FD plot for the energy is obviously just a horizontal line and the corresponding FDR is $X_e(t,t_w)=X_e^\infty=X_d^\infty=0$. This matches our findings in Sec. II B in the sense that the FD plot for the coherent observable is a straight line whose slope is the X^∞ of the incoherent observable.

3. Short-range correlated field

We have seen above that for local defect observables, the FD plot is not appropriate for determining FDT violation effects, since it converges to a straight line in the aging limit. It turns out that the same holds for defect observables defined by short-range correlated fields. To see this, we recall from Eq. (13) that, e.g., the correlation function $C(t,t_w)$ of the observable is a weighted sum of the nonlocal defect correlations, and focus on the regime $\Delta t=O(1)$ that dominates the FD plot for large t_w or t. From Eq. (20), one then easily shows that whenever a nonlocal term with given $n\neq 0$ is of the same order as the local contribution $C_d(t,t_w)\equiv C_0(t,t_w)\sim 2/\sqrt{\pi t_w}e^{-\Delta t}I_0(\Delta t)$, it can be written as

$$C_n(t,t_w)\sim\frac{2}{\sqrt{\pi t_w}}\,e^{-\Delta t}I_n(\Delta t). \tag{51}$$

In the same regime, the expression for the nonlocal susceptibility $\chi_n(t,t_w)$ is identical apart from a minus sign. This shows that, whatever the short-ranged field correlations q_n, the FD plot of $\chi(t,t_w)$ versus $C(t,t_w)$ for the observable considered becomes trivial for long times, just as in the case $q_n=\delta_{n,0}$. We, therefore, focus on the FDR in the following,

which requires analysis of $(\partial/\partial t_w)C(t,t_w)$ and the response $R(t,t_w)=-(\partial/\partial t_w)\chi(t,t_w)$ and should become nontrival in the aging limit.

By analogy with the results presented in Sec. II B 3 for spin observables, we will show that the FDR becomes identical to that for the incoherent functions in the aging limit. The procedure is again to prove that the Fourier transforms of the defect functions $(\partial/\partial t_w)C(k;t,t_w)$ and $R(k;t,t_w)$ are representations of $\tilde{\delta}$ in the aging limit and with appropriate normalization.

Expressions (B3) for $C(k;t,t_w)$ and the one that follows from Eq. (B4) for $R(k;t,t_w)$ are rather complicated and it is *a priori* not clear how they behave as times diverge. Asymptotic expansions in the aging limit $t,t_w\to\infty$ with $\epsilon \leqslant t_w/t\leqslant 1-\delta$ fixed $(\epsilon,\delta>0)$ and $|k|\leqslant K$ where $K=c/\sqrt{t_w}$ ($c>0$ arbitrarily large but finite), however, capture the relevant features of $C(k;t,t_w)$, $R(k;t,t_w)$ and have a considerably simpler form:

$$C(k;t,t_w)\sim\frac{4}{\sqrt{\pi}}\left\{\frac{1}{\sqrt{t}}e^{-k^2(t^2-{t_w}^2)/(4t)}-\frac{1}{\sqrt{t+t_w}}e^{-k^2(t+t_w)/4}\right\}+2ke^{-k^2(t+t_w)/2}\left\{\mathrm{erfi}\left(k\frac{t+t_w}{2\sqrt{t}}\right)-\mathrm{erfi}\left(k\frac{\sqrt{t+t_w}}{2}\right)\right\},\tag{52}$$

$$R(k;t,t_w)\sim\frac{1}{\sqrt{\pi t}}\left(\frac{t_w}{t}\right)k^2e^{-k^2(t^2-{t_w}^2)/(4t)}.\tag{53}$$

$\mathrm{erfi}(x)$ is the error function with imaginary argument: $\mathrm{erfi}(x)=(1/i)\mathrm{erf}(ix)$ [42]. Note that the arguments of all exponentials and the erfi's are of $O(1)$ if t_w/t and k are in the specified range. For $|k|$ larger than $O(1/\sqrt{t_w})$, results (52) and (53) do not apply.

In Eq. (52), the growth of $\mathrm{erfi}(x)\sim e^{x^2}/(\sqrt{\pi}x)$ is overcompensated by the exponential prefactor and so we can make $C(K;t,t_w)$ arbitrarily small by increasing c. For larger k, $|k|>K$, the values of $C(k;t,t_w)$ as given by Eq. (B3) also turn out to be insignificant. Therefore, $C(k;t,t_w)$ develops an infinitely sharp peak of width $O(1/\sqrt{t_w})$ at $k=0$ in the aging limit and becomes a realization of $\tilde{\delta}(k)$ when normalized by $C_d(t,t_w)$, in analogy with Eq. (33). Differentiating Eq. (52) with respect to t_w turns out to reproduce the rigorous expansion for $(\partial/\partial t_w)C(k;t,t_w)$ and similar arguments apply. Hence, $C(t,t_w)\sim N_cC_d(t,t_w)$ and $(\partial/\partial t_w)C(t,t_w)\sim N_c(\partial/\partial t_w)C_d(t,t_w)$ for any short-range correlated field with $N_c\neq 0$.

Expansion (53) for the response function $R(k;t,t_w)$ also peaks sharply in the region $|k|\leqslant K$ near $k=0$; it follows from Eq. (B4) that outside this k range, $R(k;t,t_w)$ is insignificantly small again. We have, however, $R(0;t,t_w)=0$ at all times. Nevertheless, $R_d(t,t_w)$ yields normalization and the ratio of both vanishes in the aging limit for any $k\neq 0$ (modulo 2π). So $R(k;t,t_w)$ becomes a realization of $\tilde{\delta}(k)$ when normalized by $R_d(t,t_w)$, i.e., two infinitely sharp peaks at 0^+ and 0^-. Therefore $R(t,t_w)\sim N_cR_d(t,t_w)$ for any short-range correlated field with $N_c\neq 0$.

Since $R(t,t_w)\sim N_cR_d(t,t_w)$ and $(\partial/\partial t_w)C(t,t_w)\sim N_c(\partial/\partial t_w)C_d(t,t_w)$, any defect observable O_d with short-range correlated fields ϵ_i and $N_c\neq 0$ ultimately gives the same FDR as the incoherent functions. The scaling of the peaks in Eqs. (52) and (53) implies associated time-dependent length scales in real space. As in the spin-observable case, the FDR will thus display a crossover (see Fig. 5) when these length scales become comparable with the length over which the fields ϵ_i are correlated. We note finally that, in contrast to the response $R_n(t,t_w)$ discussed above, the integrated response or susceptibility $\chi_n(t,t_w)$ displays somewhat unusual behavior; e.g., the local value $\chi_0(t,t_w)$ dominates the nonlocal terms for all times, so that to leading order there is no real-space length scale associated with the defect susceptibility. One also finds nontrivial features in the FD plots and FDRs for the cross correlations $C_n(t,t_w)$ and susceptibilities $\chi_n(t,t_w)$ [47]. However, in the aging limit and for any fixed $n\neq 0$ the FDR for the local observable $(n=0)$ is recovered as in the spin-observable case.

4. Infinite-range correlated field

We next consider the FDR for observables defined by infinite-range correlated fields. As for short-range correlated fields, we will not discuss the integrated quantities $C(t,t_w)$ and $\chi(t,t_w)$ in detail. One finds again that these give a trivial FD plot for long times, although the argument for this is somewhat more subtle than in Eq. (51) because one needs to consider an infinite range of distances n.

The exact expressions for the two-time correlation functions and susceptibilities for defect observables with power-law covariances follow from Eq. (23) by substitution of $C(k;t,t_w)$, Eq. (B3), $\chi(k;t,t_w)$, Eq. (B4), and $q_P(k)$, Eq. (25). The response $R(t,t_w)$ is then obtained from $\chi(t,t_w)$ by $R(t,t_w)=-(\partial/\partial t_w)\chi(t,t_w)$ as usual. The resulting equations are rather bulky and too complex for a meaningful discussion. So we immediately turn to the aging limit, where we can use the following, asymptotically exact, approximations. First, we replace the exact expressions in Eq. (23) for $C(k;t,t_w),R(k;t,t_w)$ by Eqs. (52) and (53). Although Eqs. (52) and (53) do not hold outside the range $k\in[-K,+K]$, the contributions to the k integrals are subleading. Second, as the integrands have infinitely sharp peaks at $k=0$ in the aging limit, we may replace $q_P(k)$ by the leading term of its expansion at $k=0$, i.e., replace $\sin(k/2)$ by $k/2$ in Eq. (25). This in turn allows us to extend the limits of integration in (23) from $-\pi,+\pi$ to $-\infty,+\infty$, whereby we again just accumulate subleading errors. Having made these approximations, which still yield asymptotically exact results, the k integrations can be evaluated and we get

$$C_P(t,t_w)\sim\frac{2}{\pi}\Gamma\left(\frac{1+\alpha}{2}\right)\left\{t^{(\alpha-1)/2}(t^2-{t_w}^2)^{-\alpha/2}-(t+t_w)^{-(1+\alpha)/2}F\left(\alpha;\frac{t+t_w}{2t}\right)\right\},\tag{54}$$

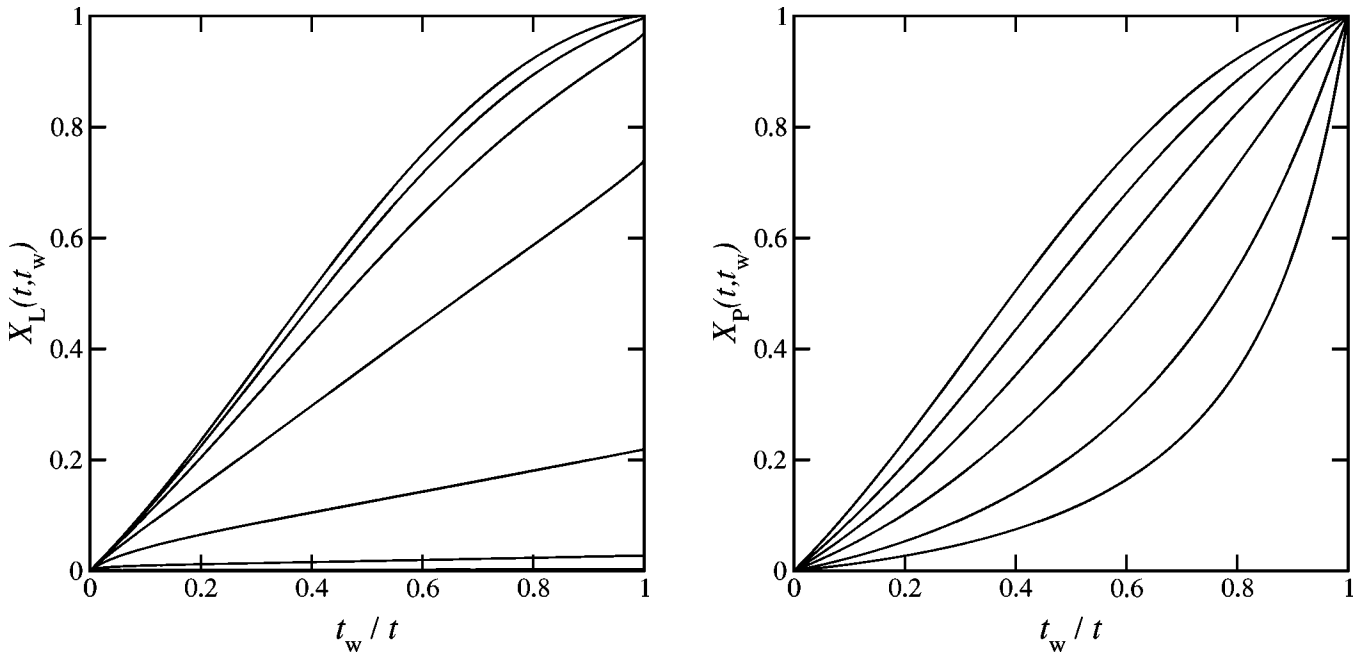

FIG. 5. Left: Time evolution of the defect-observable FDR for a random field with Lorentzian covariances (24) and $a=10^2$, correlated over $N_c = a\pi \coth a\pi \approx a\pi$ sites. For each curve t_w is kept fixed, varying over the range $t_w = 10^0, \ldots, 10^6, \infty$ from bottom to top. The curves for $t_w = 10^0, 10^1, 10^2$ are flat; in this regime, the observable is effectively identical to the energy. For $t_w = 10^3, 10^4, 10^5, 10^6$ we see the crossover to the limit curve for $t_w \to \infty$ given by Eq. (48) and corresponding to the incoherent observable. Right: Limit curves of the FDR vs t_w/t for $t, t_w \to \infty$. From bottom to top, these correspond to power-law covariances with exponent $\alpha = 0.1, 0.2, 0.4, 0.6, 0.8$. The top curve shows the random-field limit $\alpha \to 1$ for power laws, and also applies to any short-range correlated field, Sec. II C 3, with $N_c \neq 0$ or, in the extreme case, the incoherent functions of Sec. II C 1.

$$R_P(t,t_w) \sim \frac{2}{\pi}\alpha\Gamma\left(\frac{1+\alpha}{2}\right) t_w t^{(\alpha-1)/2} (t^2 - t_w^2)^{-(1+\alpha/2)}, \tag{55}$$

where we have introduced the shorthand

$$F\left(\alpha; \frac{t+t_w}{2t}\right) = 1 - (1-\alpha)2^{-(1+\alpha)/2}\left[B\left(\frac{1}{2}, 1-\frac{\alpha}{2}; \frac{t+t_w}{2t}\right) - B\left(\frac{1}{2}, 1-\frac{\alpha}{2}; \frac{1}{2}\right)\right]. \tag{56}$$

In the limit $\alpha \to 1$, Eqs. (54) and (55) reduce to the asymptotic expansions of the incoherent functions $C_d(t,t_w)$, $R_d(t,t_w)$ while $\alpha \to 0$ gives the asymptotic expansions of the coherent ones, i.e., $C_e(t,t_w)$ from Eq. (54) and $R_e(t,t_w) = 0$ from Eq. (55). So the power-law covariances (25) again allow us to interpolate between local and global observables. For intermediate exponents $0 < \alpha < 1$, the two-time correlations in O_d decrease as ${t_w}^{-1/2}\Delta t^{-\alpha/2}$ in the regime $1 \ll \Delta t \ll t_w$ and cross over to $t_w \Delta t^{-(3+\alpha)/2}$ for $1 \ll t_w \ll \Delta t$. The response $R_P(t,t_w)$ behaves as ${t_w}^{-1/2}\Delta t^{-(2+\alpha)/2}$ for $1 \ll \Delta t \ll t_w$ and $t_w \Delta t^{-(5+\alpha)/2}$ for $1 \ll t_w \ll \Delta t$. An aging expansion for the FDR again gives nontrivial curves. The derivative $(\partial/\partial t_w) C_P(t,t_w)$ follows correctly by differentiating expansion (54) which, together with Eq. (55), yields

$$X_P(t,t_w) \sim \left\{1 + \frac{t-t_w}{t_w}\left[\frac{1-\alpha}{2\alpha} + \frac{1+\alpha}{2\alpha}\sqrt{\frac{t}{t+t_w}}\left(\frac{t-t_w}{t}\right)^{\alpha/2} \times F\left(\alpha; \frac{t+t_w}{2t}\right)\right]\right\}^{-1}. \tag{57}$$

The FDR $X_P(t,t_w)$ is a function of t_w/t only and interpolates between the FDR (48) for the local defect observables ($\alpha \to 1$) and $X_e(t,t_w) = 0$ for the energy ($\alpha \to 0$). For any power $0 < \alpha < 1$, Eq. (57) crosses over from $X_P(t,t_w) = 1$ for $\Delta t \ll t_w$ to $X_P(t,t_w) = X_P^\infty = 0$ for $\Delta t \gg t_w$ (see Fig. 5).

5. Harmonically correlated fields and X^∞

In contrast to spin observables, it appears that for defect observables O_d we generically find $X^\infty = 0$. To prove this claim we may again follow the approach presented in Sec. II B 5. Introducing a FDR for defect Fourier modes $X(k;t,t_w)$ according to Eq. (40) based on the two-time defect correlation function (B3) and susceptibility (B4) allows us to write the FDR for any defect observable in form (41). The full expression for $X(k;t,t_w)$ is rather complicated and, in contrast to Eq. (42), retains a nontrivial dependence on k, t, and t_w. The only general features are $X(0;t,t_w) = 0$, since $X(0;t,t_w) = X_e(t,t_w) = 0$, and $X(\pm\pi;t,t_w) = 1 + O(\sqrt{t_w} e^{-4t_w})$ being independent of t and close to 1 for $t_w \gg 1$. For intermediate values $0 < |k| < \pi$, the FDR $X(k;t,t_w)$ can, in fact, take arbitrarily large values for appropriate t_w and t. To repeat the argument of Sec. II B 5, how-

ever, we just have to be able to take the limit $t\to\infty$ for fixed and finite t_w. A scaling analysis of $(\partial/\partial t_w)C(k;t,t_w)$ as obtained from Eq. (B3) shows that this quantity develops an infinitely sharp peak at $k=0$. Hence, the normalized distribution of $q(k)(\partial/\partial t_w)C(k;t,t_w)$ over $-\pi\leqslant k\leqslant\pi$ becomes, for sufficiently well-behaved functions $q(k)$, a realization of $\tilde{\delta}(k)$ as $t\to\infty$. Remarkably, the FDR for defects $X(k;t,t_w)$ approaches a simple, smooth function on $\pi<k<\pi$ in the same limit,

$$\lim_{t\to\infty}X(k;t,t_w)=2\left(\sin^2\frac{k}{4}\right)\left(1+4t_w\cos^2\frac{k}{4}\right)\times(2-e^{-4t_w\sin^2 k/4})^{-1}. \tag{58}$$

Together, these two facts imply that out of the spectrum of FDRs $X(k;t,t_w)$ for Fourier modes k, the long-time limit $t\to\infty$ again selects the contributions associated with infinite length scales $(k=0)$. These are, in the limit, given by Eq. (58) and equal to zero. The FDR (41) for defect observables $X(t,t_w)\to 0$ thus vanishes as $t\to\infty$ regardless of the choice of $q(k)$, except in pathological cases as discussed in Sec. II B 5. Note that because Eq. (58) for $k=0$ gives a vanishing result for any t_w, one in fact has $\lim_{t\to\infty}X(t,t_w)=X^\infty=0$, without needing to take $t_w\to\infty$.

We note finally that the behavior at short wavelengths is rather more complex for defect observables than for spins. In particular, even for what one might expect to be ''equilibrated'' wavelengths, $k^2t_w\gg 1$, it is not true that $X(k;t,t_w)\approx 1$ for all times t, and X deviates significantly from this simple value for large time differences $\Delta t\gg t_w$ as can be seen from Eq. (58).

D. Physical discussion

We saw above that apart from pathological exceptions all spin and defect observables give *identical* values for the asymptotic FDR X^∞, with $X^\infty=1/2$ for spin observables and $X^\infty=0$ for defect observables. These slopes are most easily read off from the FDT plots for the coherent observables (magnetization and energy, respectively) which become straight lines in the long-time limit.

It is natural to ask how these results would extend to observables other than those we have considered, such as $O=\Sigma_i\epsilon_i s_i s_{i+2}$ which involves spin pairs at distance 2. We have worked out explicitly the FD properties based on the general solutions given in Ref. [39] for the coherent and incoherent versions for this observable [47]; one finds that they are, up to subdominant corrections, identical to those for $O=2\Sigma_i\epsilon_i s_i s_{i+1}$. The physical interpretation is simple: $s_i s_{i+2}=-1$ if there is exactly one domain wall between spins i and $i+2$, while $s_i s_{i+2}=1$ if there is no domain wall or if there are two. The last alternative, however, is suppressed in the aging limit where typical distances between domain walls scale as $\sqrt{t_w}$, and so $s_i s_{i+2}\approx s_i s_{i+1}+s_{i+1}s_{i+2}-1$. For the coherent observable $(q_n=[\epsilon_i\epsilon_{i+n}]=1)$, this directly explains our observation; for the incoherent version $(q_n=\delta_{n,0})$, it follows from the fact that the correlations of $s_i s_{i+1}$ and $s_{i+1}s_{i+2}$ are identical to the autocorrelations of $s_i s_{i+1}$ in the aging limit.

By a similar reasoning, we can now predict the FD behavior of higher-order observables of the form

$$O_j^{(k)}=\sum_i \epsilon_i\prod_{\eta=1}^{k} s_{i+j_\eta}, \tag{59}$$

with $k\geqslant 3$ and $j_1=0$; $j_2,\ldots,j_k$ specify the relative displacements of the spins in the kth-order products. For even k, each term $\Pi_\eta s_{i+j_\eta}$ again has a sign depending on the number of domain walls between spins i and $i+j_k$. In the aging limit, configurations where more than one domain wall occurs can be neglected, so that we can replace the product by $s_i s_{i+j_k}$. By the same argument as above, this is essentially equivalent to $j_k s_i s_{i+1}$ and so should again give $X^\infty=0$.

For odd k, on the other hand, the sign of $\Pi_\eta s_{i+j_\eta}$ is essentially determined by the sign of the domain which the spin s_i finds itself in. The leading contribution is now given by configurations with no domain walls between s_i and s_{i+j_k}. Configurations with at least one domain wall are again suppressed in the aging limit. We can, therefore, replace the product simply by s_i to leading order, giving an asymptotic FDR of $X^\infty=1/2$ as for genuine first-order spin observables.

The fact that observables of even and odd order behave in different ways can also be motivated mathematically from the hierarchy of the equations obeyed by the multispin-correlation functions where the even and odd orders k turn out to decouple completely [39]. This is a peculiarity of the one-dimensional Ising model, whereas in the generic case one would expect all levels of the hierarchy to couple to each other, resulting in a unique value of X^∞. We indeed find strong evidence for this in the two-dimensional case below.

From a more physical point of view, the existence of two different values of X^∞ could be related to the fact that in the one-dimensional chain at $T=0$ one has both a critical point and an ordered phase. The result $X^\infty=0$ for defect observables could thus be related to the ordinary results for coarsening in $d\geqslant 2$ after a quench to an ordered phase, while $X^\infty=1/2$ for the spins would reflect the critical aspects of coarsening at $T=T_c=0$.

It might be interesting—though rather complicated—to use the methods described above and in Ref. [39] to study higher-order observables different from Eq. (59) for which the above leading order approximations do not apply, for example, $1-s_i s_{i+1}-s_{i+1}s_{i+2}+s_i s_{i+2}$, which corresponds to a quadratic operator in bond variables, $4b_i b_{i+1}$. We are currently exploring this issue.

To recap, the central result of this section is that (almost) all observables of form (59) interpolate between an equilibriumlike behavior with $X=1$ and an asymptotic FDR X^∞. The latter are given by the values of $X(k\to 0)$, as was argued in Refs. [33–35]. We have shown that the most efficient way of extracting X^∞ is by studying coherent functions. These results motivate the following section where the $2d$ Ising model is studied at criticality.

III. THE $2d$ ISING MODEL

In this section, we report on numerical simulations of the $2d$ Ising model. It is defined by the Hamiltonian

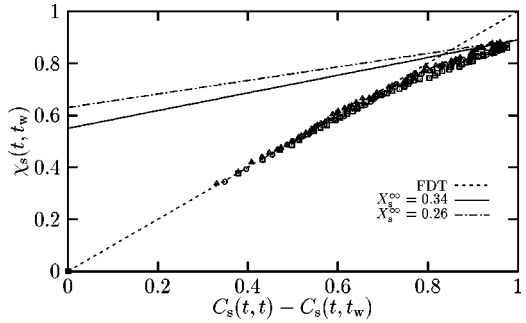

FIG. 6. FD plots for spin autocorrelation and response. Three waiting times, $t_w=43$, 179, and 460, are represented by squares, circles, and triangles, respectively. The dashed line with slope 1 shows the equilibrium FDT. The full and dash-dotted lines have slopes $X_s^\infty=0.34$ and $X_s^\infty=0.26$, respectively; these are discussed in the text.

$$\mathcal{H}=-\sum_{\langle i,j\rangle} s_i s_j, \tag{60}$$

where s_i $(i=1,\ldots,N)$ are N Ising spins located on the sites of a square lattice with periodic boundary conditions and linear size L; the sum is over nearest neighbor pairs. We perform Monte Carlo simulations using a standard Metropolis algorithm where the spins are randomly updated. One Monte Carlo step represents N attempts to flip a spin.

The system is prepared in a random state, corresponding to an infinite initial temperature. It is then quenched at $t=0$ to the critical temperature $T_c=\frac{1}{2}\ln(1+\sqrt{2})$. As stated in Sec. I D, we focus on the four natural FD relations for the Ising model, constructed from the coherent and incoherent dynamical functions of spin and defect observables. The system size we use is different for coherent and incoherent objects. Incoherent objects reflect the behavior of individual spins or defects, and simulating a very large system is advantageous in that it makes an average over many initial conditions unnecessary. Coherent objects such as $C_e(t,t_w)$ or $C_m(t,t_w)$, on the other hand, have an amplitude of the order of $1/N$. One should thus simulate many initial conditions of the smallest possible system, with the opposite constraint that the system has to be out of equilibrium even for the largest simulated time scale t_{simu} giving the condition $\xi(t_{simu})\ll L$. Our results are obtained with $t_{simu}=10^5$, $L=300$ for coherent functions, and $L=500$ for incoherent ones. Only a few samples over initial conditions are necessary for incoherent correlation functions, while 1000 initial conditions were sampled for coherent ones. This is also the number of realizations necessary to get the four susceptibilities we have computed.

We now describe our results, starting with spin observables and then turn to defect observables.

A. Spin observables

The two-time scaling behavior of the incoherent spin functions $C_s(t,t_w)$ and $\chi_s(t,t_w)$ has been the subject of a number of publications, as described in Sec. I C. We refer to the references cited there and directly present in Fig. 6 the FD plot for the spin autocorrelation and susceptibility. A very similar FD plot has been reported in Ref. [29], although a somewhat different susceptibility $\int_0^{t_w} d\tau R_s(t,\tau)$ was plotted there, so that the FD plot looks reversed compared to Fig. 6. Otherwise, we find the features anticipated in Sec. I C. The FD plot is characterized by an initial part which follows the equilibrium FDT, corresponding to short, equilibrated length scales. For larger time differences, the FD plot deviates from the FDT in a nontrivial manner due to the nonequilibrated fluctuations at small wave vectors. In the limit of large time differences the FD plot has a nonzero slope X_s^∞, in contrast to the zero slope obtained below the critical point [7,8]. These features make the FD plot rather similar to the one obtained in $d=1$, see Fig. 2 (left). Note also that a clear t_w dependence remains in these FD plots, the nonequilibrium part becoming smaller for larger t_w [29,32]. This implies, in particular, that Eq. (6) does not hold and that the FD plot we use, with $t-t_w$ instead of t_w as the curve parameter, does not directly give the FDR, as explained in Sec. I A. However, as thoroughly discussed in Ref. [29], X_s^∞ can still be read off from the FD plot, due to the asymptotic scaling of the correlation and response functions, as reviewed in Sec. I C.

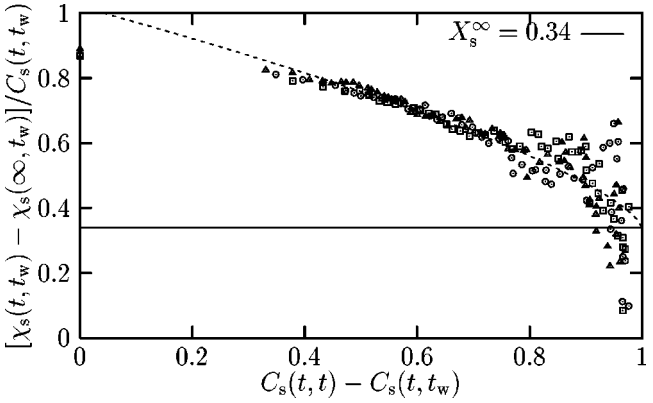

FIG. 7. Tentative extrapolation of the infinite-time slope of the FD plots of Fig. 6. The lines are only suggestive, indicating that an asymptotic FDR of $X_s^\infty=0.34$ is compatible with the data in the regime $C_s(t,t)-C_s(t,t_w)\approx 1$. The different symbols have the same meaning as in Fig. 6.

The infinite-time value for the slope of the FD plot for the $2d$ Ising model was estimated in Ref. [29] as $X_s^\infty=0.26$. We recognize from Fig. 6 that the crossover from $X=1$ to $X_s^\infty<1$ takes place over a very small range of the correlator, and that a precise determination of the infinite-time value of the FDR is difficult. A tentative numerical extrapolation is shown Fig. 7, where the quantity $[\chi_s(t,t_w)-\chi_s(\infty,t_w)]/C_s(t,t_w)$ is plotted against $C_s(t,t)-C_s(t,t_w)$; as the abscissa approaches 1 (i.e., for large time differences), the ordinate should converge to X_s^∞. The figure shows that the value $X_s^\infty=0.34$ is compatible with the data, but even though we use larger waiting times than in Ref. [29] there is substantial scatter in the points. However, we have more precise estimates of X_s^∞ to guide us, as we now describe.

The study of the model in $d=1$ in Sec. II showed that the crossover from $X=1$ to X_s^∞ for spin functions reflected the different dynamics of large and small wave vectors which for

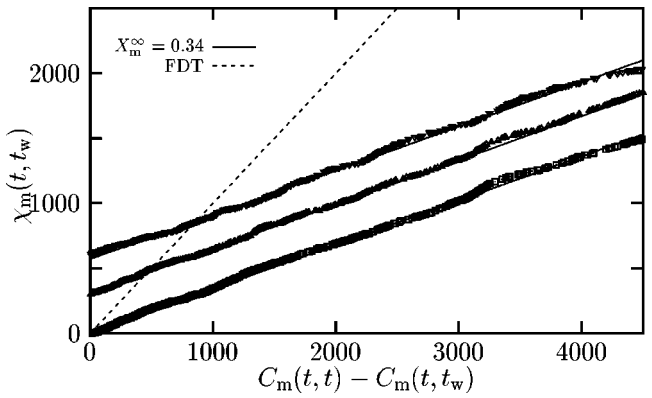

FIG. 8. FD plots of correlation and susceptibility for the magnetization. The three curves are for waiting times $t_w = 46$, 193, and 720 (bottom to top). The curves for $t_w = 193$ and $t_w = 720$ have been shifted vertically for clarity, since they would otherwise overlap with the curve for $t_w = 46$; the unshifted curves all pass through the origin as they should. The dashed line is the equilibrium FDT. The full lines have slope $X_m^\infty = 0.34$.

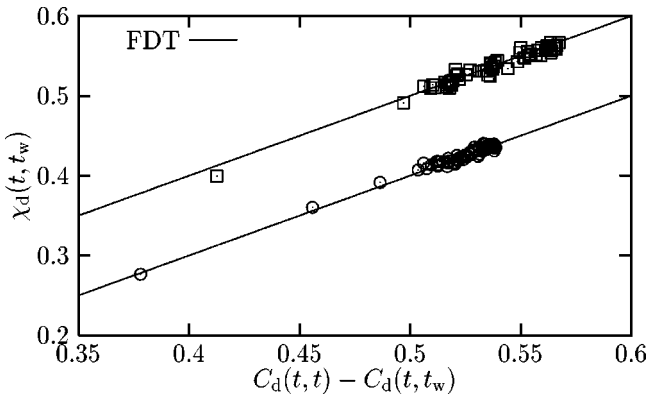

FIG. 9. FD plots for defect autocorrelation and susceptibility. Data for two waiting times, $t_w = 43$ (squares) and $t_w = 179$ (circles), are presented. The second one has been vertically shifted for clarity. The full lines represent the equilibrium FDT.

the $d = 2$ case would be defined according to $k\xi(t_w) \lesssim 1$. The dynamical behavior of the small wave vectors was governed by the asymptotic FDR X_s^∞. This suggests that a much simpler measurement of X_s^∞ should be possible by focusing on the $k \to 0$ limit, i.e., by measuring the correlation and susceptibility of the magnetization density $m(t)$. The resulting FD plot is reported in Fig. 8. As for the $1d$ case, a very simple result is obtained, with the FD plot extremely well fitted by a simple straight line. The fit holds for several decades of time, $t_w < t < t_{simu}$, for each waiting time t_w that we have considered, providing strong evidence that $X_m(t,t_w) = X_m^\infty$ at all times. Furthermore, the slopes of the three curves in Fig. 8 are very close to one another, and this allows us to report the value

$$X_m^\infty = 0.340 \pm 0.005. \tag{61}$$

This is the value we used to fit the data for the incoherent spin functions in Figs. 6 and 7, demonstrating that the data are consistent with the equality $X_s^\infty = X_m^\infty$. This is somewhat different from the value reported in Ref. [29], but we believe that our measurement from the magnetization is much more reliable than the extrapolation of the incoherent spin functions, as explained above. We note also that this value is in extremely good agreement with the two-loop expansion value reported in Ref. [33]. However, unlike the $1d$ case, we do not have a simple physical argument to explain the actual numerical value.

B. Defect observables

We now turn to defect observables. The simplest functions to consider are the defect autocorrelation function and the conjugate susceptibility. These quantities have been studied recently for kinetically constrained Ising models (in particular, the Fredrickson-Andersen model in $1d$), where they were shown to give rise to simple FD plots [36]. We present the corresponding FD plot for the $2d$ Ising model in Fig. 9. Again an apparently very simple result is obtained, with the FD plot very well fitted by the equilibrium straight line with $X = 1$. This is an unexpected result, since the system is far from equilibrium as was demonstrated by the study of spin observables in the preceding section. It could also be taken to imply, as in Ref. [36], that the asymptotic value of the FDR associated with the defects has the equilibrium value $X_d^\infty = 1$.

Our above study of the $1d$ model again clarifies the situation. There, we found that the incoherent dynamical functions of the defects exhibited a crossover from equilibrium to nonequilibrium behavior, but that the nonequilibrium part was barely visible in a FD plot, since the crossover occurs when correlators have already decayed to very small values. This suggests that the apparent equilibrium behavior observed in simulations for the $2d$ Ising and $1d$ Fredrickson-Andersen models is simply a good approximation to numerical data, but may miss nontrivial FD relations at large times due to limitations in the numerical analysis. However, as for the spin observables, the solution to this problem is straightforward and consists in focusing on the $k \to 0$ limit. We thus investigate next the coherent functions for the defects which are the autocorrelation and susceptibility for the energy density.

The resulting FD plot for the energy density is shown in Fig. 10. As for the magnetization, very good fits by pure straight lines are obtained, implying the equality $X_e(t,t_w) = X_e^\infty$. Note, however, that these plots have more noise than the ones for the magnetization. This is due to the fact that the abscissa now involves a genuine connected correlator, in which the nonzero average of the energy density needs to be subtracted off. Nonetheless, the slopes of the FD plots in Fig. 10 are very close to one another and give the result

$$X_e^\infty = 0.33 \pm 0.02. \tag{62}$$

An important outcome of this paper is that this value is compatible, within error bars, with the value reported above for the asymptotic FDT for the magnetization and the spins. This strongly suggests that the various infinite-time FDRs that we have measured in the $2d$ Ising model are all equal,

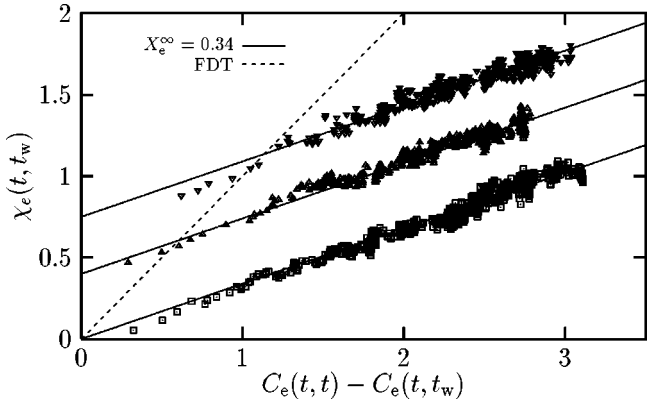

FIG. 10. FD plots for the energy density. The three curves are for $t_w = 80, 193, 464$ (bottom to top). The curves for $t_w = 193$ and $t_w = 464$ have been vertically shifted for clarity, and would otherwise again pass through the origin. The dashed curve is the equilibrium FDT; the full lines have slope $X_e^\infty = 0.34$.

and that the critical point of the $2d$ Ising model is described by a single new universal quantity

$$X_s^\infty = X_m^\infty = X_d^\infty = X_e^\infty \equiv X^\infty \approx 0.340. \tag{63}$$

SUMMARY AND DISCUSSION

In this paper, we have studied the relation between two-time multispin correlation and response functions in the nonequilibrium critical dynamics of Ising models, analytically in the $d=1$ case, and numerically in $d=2$. We have shown that FDRs, while observable dependent, fall into well-defined classes, which are qualitatively similar to those observed in various glassy systems. All FDT violations can be understood by considering separately the contributions from large wave vectors, which are at quasiequilibrium and obey the FDT, and from small wave vectors where a generalized FDT holds with a nontrivial fluctuation-dissipation ratio $X^\infty = X(k \to 0)$. In $d=1$, we find through exact calculations $X^\infty = \frac{1}{2}$ for spin observables and $X^\infty = 0$ for defect observables. In $d=2$, we find numerically a unique $X^\infty \simeq 0.34$ for all observables. These results suggest that the definition of an effective temperature $T_{\rm eff} = T/X^\infty$ for large length scales is generically possible in nonequilibrium critical dynamics.

Further, this work also suggests many interesting lines for future investigation. An important question is what are the limiting FDRs in diffusive models that are analogous to the $d=1$ Ising model but have glassy features, for example, the one-spin facilitated Fredrickson-Andersen model [48] or symmetric plaquette models [36]. Also, it would be interesting to confirm our results for the $2d$ Ising model by analyzing higher-order correlation functions by means of the renormalization group techniques used in Refs. [33–35] to confirm the uniqueness of the FDR. This would make this function an interesting quantity to study in more generic nonequilibrium situations such as driven interfaces or driven diffusive systems.

ACKNOWLEDGMENTS

We acknowledge financial support from Österreichische Akademie der Wissenschaften and EPSRC Grant No. 00800822 (P.M.), The European Community (Marie Curie Grant No. HPMF-CT-2002-01927), CNRS and Worcester College, Oxford (L.B.), EPSRC Grant No. GR/R83712/01 (L.B. and J.P.G.), the Glasstone Fund (J.P.G.), and Nuffield Grant No. NAL/00361/G (P.S.). Numerical results were obtained on OSWELL at the Oxford Supercomputing Center, Oxford University, UK.

APPENDIX A: MODIFIED BESSEL FUNCTIONS

Here we briefly summarize the main properties of the modified Bessel functions $I_n(x)$ that are relevant for the analysis given above. A comprehensive description may be found in Ref. [42]. For integer order n, $I_n(x)$ has the integral representation

$$I_n(x) = \int_0^\pi \frac{d\varphi}{\pi} \cos(n\varphi) e^{x \cos\varphi}, \tag{A1}$$

from which the functional relations

$$\frac{\partial}{\partial x} I_n(x) = \tfrac{1}{2}[I_{n-1} + I_{n+1}](x)$$

and

$$\frac{2n}{x} I_n(x) = [I_{n-1} - I_{n+1}](x) \tag{A2}$$

follow immediately. In particular, it is clear from Eq. (A1) that $I_{-n}(x) = I_n(x)$ and $I_n(-x) = (-1)^n I_n(x)$. The aging expansions of our results are based on the asymptotic formula

$$I_n(x) = \frac{e^x}{\sqrt{2\pi x}} \left[1 + \frac{1-4n^2}{8x} + O\left(\frac{1}{x^2}\right) \right], \tag{A3}$$

which applies in the limit of large arguments x for fixed order n. For the derivation of the Fourier transforms of the multispin correlation and response functions, we use

$$\sum_n e^{-inx} I_n(a) = e^{a \cos x}, \tag{A4}$$

$$\sum_n e^{-ink} I_{n-m}(a) I_{n+m}(a) = I_{2m}\left(2a \cos\frac{k}{2}\right), \tag{A5}$$

$$\sum_n e^{-ink} I_n(a)[I_{n+m}(b) + I_{n-m}(b)] = 2T_m\left(\frac{b + a\cos k}{A}\right) I_m(A), \tag{A6}$$

where Eqs. (A5) and (A6) follow from Eq. (A1), the well-known identity (A4) and trigonometric relations. In Eq. (A6) $0 < a \leq b$ is required, $A = \sqrt{a^2 + b^2 + 2ab\cos k}$ and the $T_n(x) = \cos(n \arccos x)$ are Chebyshev polynomials of degree n in x.

APPENDIX B: FOURIER TRANSFORMS

The Fourier transforms of spin correlation and response functions (18) and (19) follow immediately when using Eq. (A4):

$$C(k;t,t_w)=e^{-(t+t_w)(1-\cos k)}\left\{1+\int_0^{2t_w}d\tau e^{-\tau\cos k}[I_0+I_1](\tau)\right\}, \tag{B1}$$

$$\chi(k;t,t_w)=\frac{1}{2}\int_{t_w}^{t}d\tau e^{-(t-\tau)(1-\cos k)}e^{-2\tau}[I_0+2I_1+I_2](2\tau). \tag{B2}$$

For defect correlations, however, a direct transformation of Eq. (20) yields a rather intractable expression. Therefore, we first rewrite Eq. (20) using the identity (which can be verified by differentiation)

$$e^{-(t-t_w)}I_n(t-t_w)=e^{-(t+t_w)}I_n(t+t_w)-\int_{t-t_w}^{t+t_w}d\tau\tfrac{1}{2}e^{-\tau}[I_{n-1}-2I_n+I_{n+1}](\tau),$$

as

$$\begin{aligned}C_n(t,t_w)=e^{-2(t+t_w)}[I_n^2-I_{n-1}I_{n+1}](t+t_w)+\frac{1}{2}\int_{t-t_w}^{t+t_w}d\tau e^{-(t+t_w+\tau)}\\ \times\{[I_{n-1}-I_{n+1}](\tau)[I_{n-1}-I_{n+1}](t+t_w)\\ -[I_{n-1}-2I_n+I_{n+1}](\tau)[I_{n-1}+2I_n+I_{n+1}](t+t_w)\}.\end{aligned}$$

Now, utilizing Eq. (A2) and expressing factors of n as derivatives with respect to k, the Fourier series for $C(k;t,t_w)$ may be written in the form

$$\begin{aligned}C(k;t,t_w)=e^{-2(t+t_w)}\sum_n e^{-ink}[I_n^2-I_{n-1}I_{n+1}](t+t_w)-\frac{1}{2}\int_{t-t_w}^{t+t_w}d\tau e^{-(t+t_w+\tau)}\\ \times\left\{\frac{4}{\tau(t+t_w)}\frac{\partial^2}{\partial k^2}\sum_n e^{-ink}I_n(\tau)I_n(t+t_w)\right.\\ \left.+2\left(\frac{\partial}{\partial\tau}-1\right)\sum_n e^{-ink}I_n(\tau)[I_{n-1}+2I_n+I_{n+1}](t+t_w)\right\}.\end{aligned}$$

All summations in this expression can be evaluated via Eqs. (A5) and (A6). Some fairly complicated algebra is required to simplify the resulting expression, but finally one obtains the compact result

$$C(k;t,t_w)=e^{-2(t+t_w)}\frac{I_1\left(2(t+t_w)\cos\frac{k}{2}\right)}{(t+t_w)\cos\frac{k}{2}}+4\int_0^{t_w}d\tau e^{-2(t+\tau)}\left[\frac{1}{A}I_1(2A)+2\frac{t_w-\tau}{A}\sin^2\left(\frac{k}{2}\right)\left(I_1(2A)+\frac{t_w-\tau}{A}I_2(2A)\right)\right], \tag{B3}$$

where $A=\sqrt{(t+\tau)^2\cos^2(k/2)+(t_w-\tau)^2\sin^2(k/2)}$. Equation (B3) is the most convenient representation for $C(k;t,t_w)$, both for numerical and analytical purposes. The calculation of the Fourier transform of the defect susceptibility (21) is comparatively easy; from Eqs. (A5) and (A6), one finds

$$\chi(k;t,t_w)=2e^{-2t}\left\{[I_0+I_1](2t)-I_0(2A)-\frac{t\cos^2(k/2)+t_w\sin^2(k/2)}{A}I_1(2A)\right\}, \tag{B4}$$

with $A=\sqrt{t^2\cos^2(k/2)+t_w^2\sin^2(k/2)}$.

APPENDIX C: POWER-LAW COVARIANCES

Here we show that the covariances $q_{\mathrm{P},n}$ given in Eq. (25) follow a power law as $|n|\to\infty$ and establish the link $q_{\mathrm{P},n}=\mathcal{F}^{-1}\{q_{\mathrm{P}}(k)\}$. Let us first focus on the Fourier integral (22) which—since $q_{\mathrm{P}}(k)$ is even in k—may be written as

$$q_{\mathrm{P},n}=\frac{\Gamma^2\left(\frac{1+\alpha}{2}\right)}{2^{1-\alpha}\Gamma(\alpha)}\int_0^{2\pi}\frac{dk}{2\pi}\left(\sin\frac{k}{2}\right)^{\alpha-1}\cos(nk), \tag{C1}$$

where $0<\alpha<1$ as before. The simple substitution $x=k/2$ yields the solvable integral [42]

$$\int_0^{\pi}\frac{dx}{\pi}(\sin x)^{\alpha-1}\cos 2nx=\frac{(-1)^n}{\alpha 2^{\alpha-1}B\left(\frac{1+\alpha}{2}+n,\frac{1+\alpha}{2}-n\right)}. \tag{C2}$$

Using the functional relation [42] $B(x,y)=\Gamma(x)\Gamma(y)/\Gamma(x+y)$ for the beta function $B(x,y)$ and simplifying the remaining expression yield the result for $q_{\mathrm{P},n}$ given in Eq. (25). Now we turn to the asymptotic behavior of $q_{\mathrm{P},n}$ as $|n|\to\infty$. For $n\geqslant 1$ we may rewrite $q_{\mathrm{P},n}$, using $\Gamma(x)\Gamma(1-x)=\pi/\sin\pi x$ and $\Gamma(x+1)=x\Gamma(x)$, in the form

$$q_{\mathrm{P},n}=\prod_{k=0}^{n-1}\frac{1-\alpha+2k}{1+\alpha+2k}. \tag{C3}$$

It is obvious from Eq. (C3) that $q_{\mathrm{P},n}$ is monotonically decreasing and vanishes for $n\to\infty$ as long as $\alpha>0$. It is equally clear that $q_{\mathrm{P},n}=1$ for $\alpha\to 0$ and $q_{\mathrm{P},n}=\delta_{n,0}$ as $\alpha\to 1$ (since $q_{\mathrm{P},n}$ is even in n and $q_{\mathrm{P},0}=1\,\forall\,\alpha$). In order to understand the asymptotic behavior of $q_{\mathrm{P},n}$, we take the logarithm of Eq. (C3) and use the bounds

$$\int_0^n dk\,a_k\leqslant\sum_{k=0}^{n-1}a_k\leqslant a_0+\int_0^{n-1}dk\,a_k, \tag{C4}$$

which hold for any nonincreasing function a_k. For the case at hand, the integrals can be solved easily. Exponentiating the result, multiplying by n^{α}, and taking the limit $n\to\infty$ then give

$$(2e)^{-\alpha}\sqrt{\frac{(1-\alpha)^{1-\alpha}}{(1+\alpha)^{1+\alpha}}}\leqslant\lim_{n\to\infty}n^{\alpha}q_{\mathrm{P},n}\leqslant(2e)^{-\alpha}\sqrt{\frac{(1+\alpha)^{1-\alpha}}{(1-\alpha)^{1+\alpha}}}, \tag{C5}$$

which implies that there exists a finite constant c such that $q_{\mathrm{P},n}\sim cn^{-\alpha}$ for $0<\alpha<1$.

[1] L.F. Cugliandolo and J. Kurchan, Phys. Rev. Lett. **71**, 173 (1993).
[2] J.-P. Bouchaud, L. F. Cugliandolo, J. Kurchan, and M. Mézard, in *Spin Glasses and Random Fields*, edited by A.P. Young (World Scientific, Singapore, 1998).
[3] L.F. Cugliandolo, e-print cond-mat/0210312.
[4] L.F. Cugliandolo and J. Kurchan, J. Phys. A **27**, 5749 (1994).
[5] S. Franz and M. Mézard, Europhys. Lett. **26**, 209 (1994); Physica A **210**, 48 (1994).
[6] L.F. Cugliandolo, J. Kurchan, and L. Peliti, Phys. Rev. E **55**, 3898 (1997).
[7] A. Barrat, Phys. Rev. E **57**, 3629 (1998).
[8] L. Berthier, J.-L. Barrat, and J. Kurchan, Eur. Phys. J. B **11**, 635 (1999).
[9] P. Sollich, F. Lequeux, P. Hébraud, and M.E. Cates, Phys. Rev. Lett. **78**, 2020 (1997).
[10] L. Berthier, J.-L. Barrat, and J. Kurchan, Phys. Rev. E **61**, 5464 (2000).
[11] A.J. Bray, Adv. Phys. **43**, 357 (1994).
[12] Th.M. Nieuwenhuizen, Phys. Rev. Lett. **80**, 5580 (1998).
[13] S. Fielding and P. Sollich, Phys. Rev. Lett. **88**, 050603 (2002).
[14] L. Berthier and J.-L. Barrat, Phys. Rev. Lett. **89**, 095702 (2002); J. Chem. Phys. **116**, 6228 (2002).
[15] L.F. Cugliandolo, J. Kurchan, and G. Parisi, J. Phys. I **4**, 1641 (1994).
[16] L.F. Cugliandolo and D.S. Dean, J. Phys. A **28**, 4213 (1995).
[17] W. Zippold, R. Kühn, and H. Horner, Eur. Phys. J. B **13**, 531 (2000).
[18] S.A. Cannas, D.A. Stariolo, and F.A. Tamarit, Physica A **294**, 362 (2001).
[19] F. Corberi, E. Lippiello, and M. Zannetti, Phys. Rev. E **65**, 046136 (2002).
[20] G. Parisi, F. Ricci-Tersenghi, and J.J. Ruiz-Lorenzo, Eur. Phys. J. B **11**, 317 (1999).
[21] D.A. Stariolo and S.A. Cannas, Phys. Rev. B **60**, 3013 (1999).
[22] F. Corberi, E. Lippiello, and M. Zannetti, Phys. Rev. E **63**, 061506 (2001); Eur. Phys. J. B **24**, 359 (2001); F. Corberi, C. Castellano, E. Lippiello, and M. Zannetti, Phys. Rev. E **65**, 066114 (2002).
[23] M. Henkel, M. Pleimling, C. Godrèche, and J.-M. Luck, Phys. Rev. Lett. **87**, 265701 (2001).
[24] M. Henkel and M. Pleimling (unpublished); F. Corberi, E. Lippiello, and M. Zannetti, e-print cond-mat/0211609.
[25] M. Henkel, M. Paessens, and Michel Pleimling, e-print cond-mat/0211583.
[26] C. Godrèche and J.-M. Luck, J. Phys. A **33**, 1151 (2000).
[27] E. Lippiello and M. Zannetti, Phys. Rev. E **61**, 3369 (2000).
[28] G.J.M. Koper and H.J. Hilhorst, Physica A **155**, 431 (1989).
[29] C. Godrèche and J.-M. Luck, J. Phys. A **33**, 9141 (2000).
[30] C. Godrèche and J.-M. Luck, J. Phys. C **14**, 1589 (2002).
[31] P.C. Hohenberg and B.I. Halperin, Rev. Mod. Phys. **49**, 435 (1977).
[32] L. Berthier, P.C.W. Holdsworth, and M. Sellitto, J. Phys. A **34**, 1805 (2001).
[33] P. Calabrese and A. Gambassi, Phys. Rev. E **66**, 066101 (2002).

[34] P. Calabrese and A. Gambassi, Phys. Rev. B **66**, 212407 (2002).
[35] P. Calabrese and A. Gambassi, Phys. Rev. E **67**, 036111 (2003).
[36] A. Buhot and J.P. Garrahan, Phys. Rev. Lett. **88**, 225702 (2002).
[37] R.J. Glauber, J. Math. Phys. **4**, 294 (1963).
[38] A.J. Bray, J. Phys. A **23**, L67 (1989).
[39] P. Mayer and P. Sollich (unpublished).
[40] D. Bedeaux, K.E. Shuler, and I. Oppenheim, J. Stat. Phys. **2**, 1 (1970).
[41] P. Sollich, S. Fielding, and P. Mayer, J. Phys. C **14**, 1683 (2002).
[42] I. Gradstein and I. Ryzhik, *Table of Integrals, Series, and Products* (Academic Press, New York, 1980).
[43] For $t=t_w$, the integral in Eq. (18) is of the form of a Laplace convolution. A Laplace transform indeed allows one to simplify this expression and rewrite it explicitly in terms of the modified Bessel functions. This result has also been found in J.L. Spouge, Phys. Rev. Lett. **60**, 871 (1988); J.G. Amar and F. Family, Phys. Rev. A **41**, 3258 (1990).
[44] See, e.g., B. Derrida and R. Zeitak, Phys. Rev. E **54**, 2513 (1996).
[45] J.E. Santos, J. Phys. A **30**, 3249 (1997).
[46] K.P.N. Murthy and G.M. Schütz, Phys. Rev. E **57**, 1388 (1998).
[47] P. Mayer, Ph.D. thesis, King's College, London.
[48] G.H. Fredrickson and H.C. Andersen, Phys. Rev. Lett. **53**, 1244 (1984).